





# Recent Advancements in Reconfigurable mmWave Devices Based on Phase-Change and Metal Insulator Transition Materials

TEJINDER SINGH <sup>1,2</sup> (Senior Member, IEEE), GWENDOLYN HUMMEL <sup>3</sup> (Member, IEEE),  
MOHAMMAD VASEEM <sup>4</sup> (Member, IEEE), AND ATIF SHAMIM <sup>4</sup> (Senior Member, IEEE)

(Invited Paper)

<sup>1</sup>Advanced Wireless Technology R&D Group, Office of the CTO, Dell Technologies, Ottawa, ON K2B 8J9, Canada

<sup>2</sup>Department of Electrical and Computer Engineering, University of Waterloo, Waterloo, ON N2L 3G1, Canada

<sup>3</sup>Sandia National Laboratories, Albuquerque, NM 87185 USA

<sup>4</sup>CEMSE Division, King Abdullah University of Science and Technology, Thuwal 23955, Saudi Arabia

CORRESPONDING AUTHOR: Tejinder Singh (e-mail: singh.tejinder@dell.com; Tejinder.Singh@uwaterloo.ca).

This work did not involve human subjects or animals in its research.

**ABSTRACT** Chalcogenide Phase Change Materials (PCM) and metal insulator transition (MIT) materials are a group of materials that are capable of switching between low resistance and high resistance states. These emerging materials have been widely used in optical storage media and memory devices. Over the past recent years, there have been interests in exploiting the PCM and MIT materials, especially germanium antimony telluride (GST) alloys and vanadium dioxide (VO<sub>2</sub>), for radio frequency (RF) applications. The PCM and MIT-based RF devices are expected to bridge the gap between semiconductor switches and microelectromechanical system (MEMS) switches as they combine the low insertion loss performance of MEMS technology and the small size and reliability performance of semiconductor technology. This article presents an overview of the PCM and MIT materials for RF circuits and discusses the recent advancements in reconfigurable millimeter-wave (mmWave) devices based on PCM and MIT materials in depth.

**INDEX TERMS** Attenuators, delay networks, emerging technologies, germanium telluride (GeTe), MTT 70th Anniversary Special Issue, millimeter-wave (mmWave) components, MMICs, phase change material (PCM), phase shifters, RF switches, RF integrated circuits, scalable PCM switch matrices, tunable circuits.

## I. INTRODUCTION

Miniature, reliable, and high-performance radio frequency (RF) switches are needed to configure antennas, matching networks, phase shifters, filters, and multiband amplifiers in RF front-end modules. RF switches are therefore the fundamental building blocks for realizing reconfigurable front ends in wireless communication systems. For future communications, RF devices are required to meet stringent specifications of beyond 5G (B5G) networks with key enabling technologies such as, massive multiple-input multiple-output (MIMO), millimeter wave (mmWave), beamforming, full duplex, and machine to machine (M2M). Implementation of beamforming and full-duplex systems requires the use of reconfigurable RF

devices, which in turn employ tunable elements and switches. In particular, full duplex systems require the use of tunable matching networks, phase shifters, tunable attenuators, and tunable delay lines.

Traditional RF switches such as mechanical or semiconductor are used extensively. Some of the most used coaxial mechanical switches demonstrate exceptional RF performance but are bulky in size and expensive [1]. Semiconductor-based switch technologies such as solid-state CMOS, GaAs, SiGe, and SOI offer devices with miniaturized overall footprints and low-cost integration with other front-end RF modules, but they exhibit several limitations including limited RF power handling, poor linearity performance and high insertion loss

particularly at mmWave frequencies [2], [3]. In the past few years, microelectromechanical systems (MEMS)-based RF switches and components have demonstrated promising RF performance [4], [5], [6], but due to the mechanically moving micro-scale membranes, MEMS-based devices suffer from contact degradation over time, high operational voltage requirement, slow switching time, and have in general reliability and packaging limitations [7]. More recently, commercial RF MEMS switches have demonstrated improvement in reliability, but only operate up to 26 GHz [8], [9].

Phase change materials (PCM) and metal insulator transition (MIT) materials based devices are two of the most promising candidates for building low-cost and low-loss broadband microwave and mmWave components. PCM based devices offer the development of highly miniaturized and latching switches with negligible DC power consumption. PCM's property of offering more than five orders of resistance change with the application of nanosecond voltage pulses, makes this technology an ideal candidate for low-loss, high-speed switching at microwave and mmWave frequencies. PCM-based devices offer the flexibility to reduce the device area by dense integration of switching unit-cells. One of the key features of this PCM technology is its non-volatile functionality, that does not require constant DC power to hold the switch state [10], [11], [12], [13], [14], [15], [16]. Recently, various reconfigurable phase change based mmWave components have been demonstrated [17], [18], [19].

This article explores the recent advancements in the PCM and MIT materials and discusses the microwave and mmWave applications in detail. The PCM GeTe is explored at first in-depth for RF applications including the characterization, operation, and fabrication process. PCM GeTe-based RF switches and discussed in detail and their performance is compared with the current state-of-the-art. Various reconfigurable devices are presented such as a crossbar switch matrix, a phase shifter and a variable attenuator using PCM GeTe switches. Various emerging PCM materials are also explored briefly for their use in future potential reconfigurable devices. In the second half of the paper, MIT material VO<sub>2</sub> is described extensively from reconfigurable RF applications viewpoint. Devices including but not limited to RF switches, reconfigurable antennas, filters are discussed.

## II. HISTORY AND ORIGIN OF PHASE CHANGE MATERIAL (GST) AND ITS ALLOYS

While Ovshinsky [12] is generally credited as the inventor of phase change materials for information storage, the discovery of phase changing electrical characteristics dates back to the early 1900 s in the little known and seldom cited pioneering work of Alan Tower Waterman. While studying thermionic emission of certain hot salts [20], Waterman observed a large negative coefficient of resistance of the molybdenum disulfide (MoS<sub>2</sub>) with respect to temperature. More significantly, he observed a breakdown in resistivity characteristic when the device under test was heated by means of the electric current.

He pointed out that MoS<sub>2</sub> may exist in two forms,  $\alpha$  of high resistance and  $\beta$  of low resistance. The breakdown phenomenon and progressive conductivity changes are prominent of the phase change behavior in chalcogenide materials. Waterman also pointed out that the transition from  $\alpha$  form to  $\beta$  form can be initiated by heat, electric field or light. However, without the use of modern physical analysis tools such as transmission electron microscopy and X-ray crystallography, he was not able to observe any physical changes of MoS<sub>2</sub> along with the conductivity changes. He did however notice an increase in hardness with the increase in conductivity [21].

Since 1960, Ovshinsky has been working with amorphous chalcogenides. He developed both electrically controlled threshold and memory switching devices and first reported his findings in a paper published in Physical Review Letters in 1968 [12], which detailed the operations of reversible switching in memory devices composed of 48% tellurium, 30% arsenic, 12% silicon, and 10% germanium. The most significant contribution of Ovshinsky's work is the demonstrated practicality of the switching phenomenon in continuous successful switching operations of multiple devices over periods of many months. Interest in phase change memory was effectively initiated by this ground-breaking paper by Ovshinsky which remains the most cited literature in the field of phase change memory [21].

In the early 1970's, phase change memory drew a lot of interest in industry and academia with the rapid expansion of applications of computers. The most notable work was the development of a 256-bit array comprised of a 16x16 matrix of phase change memory cells by R. G. Neale and D. L. Nelson of Energy Conversion Devices along with Gordon E. Moore of Intel [22]. Their memory cell consisted of a storage element, coined as the Ovonic amorphous semiconductor switching device, in series with a silicon p-n junction diode. The Ovonic memory element comprised of a thin film of phase change material sandwiched between two molybdenum electrodes as a non-volatile bi-stable resistor. The high-to-low resistance ratio was about 10<sup>3</sup>. Another attempt to build a phase change memory device was reported by Roy R. Shanks and Craig Davis of the Burroughs Corporation. They published their results of a 1024-bit phase change memory in 1978 [21], [23].

In early 2000's, the ability of having a rewritable media was also an important requirement [24]. A landmark was achieved in the late 1980 s by Matsushita/Panasonic who developed phase-change optical disc technology that remained stable over a million use cycles [25]. This technology became the mainstream in optical disc production and in the late 1990 s leading to the commercialization of 4.7 GB digital versatile disc random access memory (DVD-RAM). During the development process, various materials were examined, and the best performing PCM in terms of speed and stability were found to be Ge<sub>2</sub>Sb<sub>2</sub>Te<sub>5</sub> (GST) for DVD-RAM and an AgInSbTe alloy for DVD-RW [26] applications. The phenomenology of phase-change optical recording is simple. An initially amorphous as-deposited GST layer is crystallized by

exposure to a laser beam of intensity sufficient to heat the material to a temperature slightly above the glass-transition temperature. A subsequent exposure to an intense and short laser pulse melts the GST that is then converted into the amorphous state on quenching. A recorded bit is an amorphized mark against the crystalline background. The reversibility of the crystallization–amorphization process allows fabrication of rewritable memory [24].

A chalcogenide phase change material GeTe based reconfigurable switch was first presented by E. Chua in 2010 [27], [28]. The switch exhibited low ON state resistance of 180  $\Omega$  and a large dynamic range of  $7 \times 10^3$ . This paper also reported a partial crystallization and partial re-amorphization model to explain the differences between the measured and calculated device in OFF and ON state resistances, respectively. Although this paper reports the switching properties of phase change material by using a phase change via, no RF parameters are reported.

Early research on using directly and indirectly heated GeTe based RF switches was presented by University of Michigan [29], Northrop Grumman Corp. [30], [31], HRL Laboratories [32], [33], University of Limoges [34], and the University of Waterloo [15], [35], [36]. Although, the PCM via started the initial motivation towards the development of high performance RF switches utilizing PCM, the four-terminal PCM switch demonstrated by Northrop Grumman Corp. [30] solves various issues associated with PCM vias for RF applications including but not limited to, high single via ON-resistance/insertion loss, partial recrystallization and amorphization, low RF breakdown, difficulty/inability to add vias in parallel to lower ON-resistance due to inconsistent switching and large amorphization current, and coincident switch control line and RF signal line, like a diode. Most of these switches have a high cut-off frequency of 10 THz to 12 THz with impressive RF performance, encouraging the development of a wide range of reconfigurable PCM-based RF components for both microwave and millimeter-meter wave applications [15], [17], [18], [19], [36], [37], [38], [39], [40], [41], [42], [43], [44], [45], [46]. One advantage of the PCM technology compared to other technologies is the ability to monolithically integrate with CMOS/BiCMOS processes to significantly increase system integration. The integration of PCM with a commercial SiGe BiCMOS process [47] and commercial RFSOI process with 1 billion cycles [48] was recently demonstrated.

The historical challenge with the RF PCM switches has been their reliability/cycle endurance. However, several efforts on the reliability aspects led by HRL Laboratories and TowerJazz Semiconductors paved the way towards the development of highly reliable RF switches. The first PCM switch with 10 million cycles was demonstrated by J. Moon et al. from HRL Laboratories [49] while N. El-Hinnawy et al. from TowerJazz Semiconductors successfully the RF PCM switch with impressive 1 billion cycles and 25 THz cut-off frequency [50].

**TABLE 1. Summary of the Measured Physical, Electrical, and Optical Constants of Amorphous and Crystalline GeTe films [10]**

Material Property	Amorphous <sup>a</sup>	Crystalline
Density (g/cc)	$5.6 \pm 0.5$	6.17
Resistivity ( $\Omega\cdot\text{cm}$ )		
at 300 K	$\sim 10^3$	$\sim 2 \times 10^{-4}$
at 77 K	$> 10^{10}$	$\approx 1.5 \times 10^{-4}$
Temp. Coeff. of Resistivity	Negative	Positive
Conductivity type (Hall)	<i>p</i>	<i>p</i>
Carrier conc. ( $\text{cm}^{-3}$ )	$\sim 10^{18}$	$10^{20} - 10^{21}$
Mobility ( $\text{cm}^2 \text{V}^{-1} \text{sec}^{-1}$ )		
at 300 K	$< 10^{-2}$	15 – 120
at 77 K	NA <sup>b</sup>	20 – 250
Susceptibility mass ( $m_s/m_e$ )	NA <sup>b</sup>	0.16 – 0.35
Fermi energy at 300 K (eV)	NA <sup>b</sup>	0.3 – 0.5
Optical gap (eV)	$\sim 0.85$	$\sim 0.73 - 0.95$
Electrical band gap (eV)	$\sim 0.8$ (intrinsic)	$\sim 0.1 - 0.2$

<sup>a</sup> Amorphous films are stable below 145 °C

<sup>b</sup> NA: Data not available

### III. PHASE CHANGE MATERIAL: GERMANIUM TELLURIDE (GETE)

GeTe is a chemical compound of germanium and tellurium and is a component of chalcogenide glasses. It shows semi-metallic conduction and ferroelectric behavior [51]. GeTe exists in three major crystalline forms, room-temperature  $\alpha$  (rhombohedral) and  $\gamma$  (orthorhombic) structures and high-temperature  $\beta$  (cubic rocksalt-type) phase;  $\alpha$  phase being the majority phase of pure GeTe below the ferroelectric Curie temperature of approximately 670 K [52]. Doped GeTe is a low temperature superconductor [53]. Table 1 summarizes the relevant measured physical, electrical, and optical constants of amorphous and crystalline GeTe films [10]. The ON (crystalline) state resistivity is  $2 \times 10^{-4} \Omega\cdot\text{cm}$  and OFF (amorphous) state resistivity is  $> 10^3 \Omega\cdot\text{cm}$ . This results in a dynamic range (OFF state/ON state resistance ratio) of around  $5 \times 10^6$ . Such values have been the driver of using GeTe for RF applications [39], [54].

Phase change (chalcogenide) material is defined as alloys containing group VI elements such as sulfur (S), selenium (Se) and telluride (Te). Alloys containing germanium (Ge), antimony (Sb) and Te are most common, with germanium-antimony-telluride ( $\text{Ge}_2\text{Sb}_2\text{Te}_5$ ) alloy being the most thoroughly researched material. Fig. 1 shows the ternary phase diagram for this system where single phase alloys that lie on the pseudo binary line of germanium telluride (GeTe) and antimony telluride ( $\text{Sb}_2\text{Te}_3$ ) are indicated. Allies include  $\text{Ge}_1\text{Sb}_2\text{Te}_4$ ,  $\text{Ge}_2\text{Sb}_2\text{Te}_5$ , and  $\text{Ge}_1\text{Sb}_4\text{Te}_7$ . Along the pseudo binary line from GeTe to  $\text{Sb}_2\text{Te}_3$ , the properties change from high stability and low speed to low stability and high speed [54]. A material composition selected from the pseudo binary line may typically achieve fast crystallization and reasonable stability.

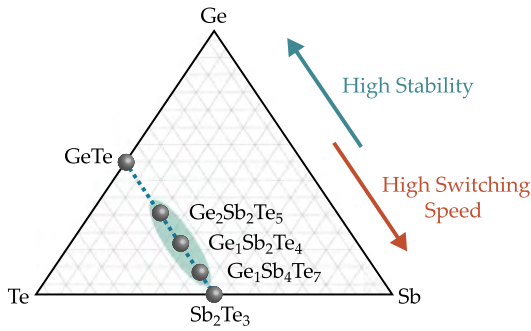


**FIGURE 1.** Ge-Sb-Te ternary phase diagram depicting various phase change alloys along with single phase compositions that reside on the tie-line of GeTe and  $\text{Sb}_2\text{Te}_3$ .

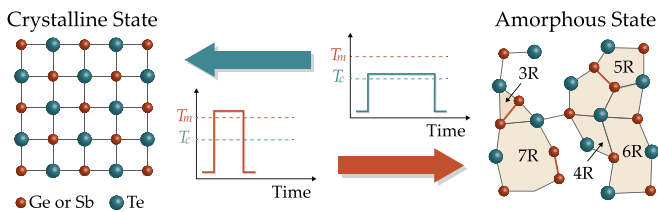


**FIGURE 2.** Reversible switching of phase change material using an electrical pulse, in non-volatile memory applications [15].

### A. PRINCIPLE OF OPERATION

The PCM has the unique property of reversible switching between amorphous and crystalline states upon specific heat treatment by means of electrical pulses. The state where atoms are arranged in a disorderly manner (short range order) is called the amorphous state, whereas the state where atoms are organized in an orderly manner (long range order) is called crystalline state. For non-volatile memory applications, the conventional principle of PCM is illustrated in Fig. 2. The large contrast in resistance between the two states is used as a form of non-volatile memory to represent two states of binary [54].

### B. FABRICATION PROCESS

The PCM-based RF devices can be fabricated on a wide range of substrates and thin films [15], [30], [42], [47], [48], [49], [55], [56], [57], [58]. An example fabrication process flow from [42] is discussed in this manuscript as shown in Fig. 3. The fabrication of the PCM-based RF switch depicted in Figure 10 involved the use of a high resistivity substrate and the deposition of GeTe films, high resistivity thin-film for the heater, dielectric layers to insulate the heater from the GeTe switching element and high conductivity metallization thin-films for the input/output ports of the switch. The micro-fabrication process starts with a RCA-1 and Piranha cleaning of high resistivity Si wafer ( $> 20 \text{ k}\Omega \cdot \text{cm}$ ) and  $500 \mu\text{m}$  thickness. The process includes eight layers with four metal layers (M0, M1, M2, and M3), one PCM layer and three dielectric layers (D0, V0, and V1). D0 is the substrate oxide for thermal isolation. M2 and M3 are used for RF signal routing and

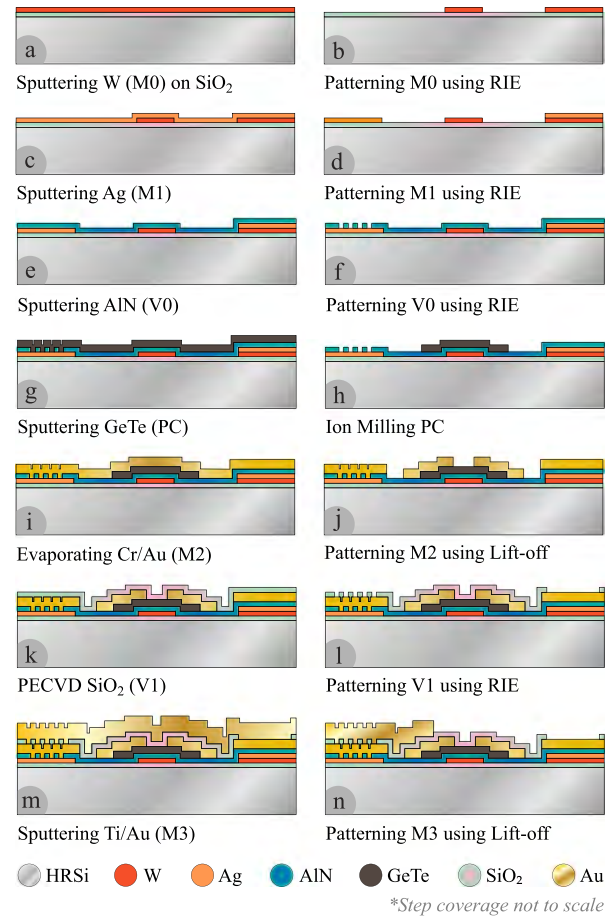


**FIGURE 3.** An example multi-layer fabrication process flow having two metal layer for RF signal routing and two metal layers for bias routing [42].

M0 layer is used for the micro-heaters while M1 is used for biasing networks that can be used for some RF components. a) 50 nm tungsten (W) is sputtered (M0) at elevated temperature of  $850^\circ\text{C}$  deposited on a thin dielectric insulator oxide layer that is b) patterned using RIE. c) 70 nm silver (Ag) is sputtered (M1) and d) patterned using RIE, followed by e) deposition of 100 nm AlN layer using RF sputtering and, f) patterned using RIE to act as a barrier layer (V0) between micro-heaters and PCM. g) 130 nm GeTe thin film is sputtered using Ge [50]:Te [50] target (PC) and, h) patterned using ion milling. i) evaporation of 350 nm of Au that serves as M2 with 30 nm of Ti as a seed layer. j) M2 is patterned using lift-off technique. k) 200 nm  $\text{SiO}_2$  layer is deposited using low temperature PECVD and, l) patterned using RIE that serves as a passivation layer for PCM (V1). m) sputtering of 450 nm Au layer (M3) with 40 nm Ti layer as a seed layer. n) M2 is patterned using lift-off technique.

Optimization of GeTe thin films is a crucial step in the development of high performance RF switches with low ON-state loss and high OFF-state isolation. Performance of the PCM switch depends on the GeTe film quality. Poor quality films exhibit lower resistance ratio between crystalline and amorphous state. Various factors including but not limited



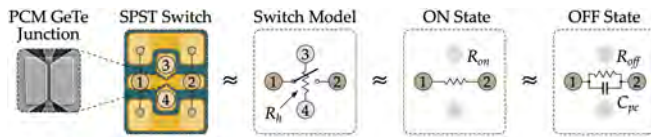


**FIGURE 4.** A four terminal phase-change RF switch. Terminals 1 and 2 are RF input and output ports while terminal 3 and 4 are bias pads to provide actuation pulse to the switch. A simplified switch model in both ON and OFF state is shown.

to deposition type, base pressure, chamber pressure, material purity, deposition power, DC/RF sputtering, inert gas flow rate, or deposition temperature can severely affect the film quality [37], [40], [42]. Issues related to the change in the PCM film quality with deposition temperature has been investigated using AFM and SEM in [15], [37]. The heated deposition both improves resistivity and eliminates cracking over surface topology.

### C. PHASE CHANGE RF SWITCHES

The GeTe material exhibits a transition between crystalline (ON) and amorphous state (OFF) that is attained by heating the PCM above its melting temperature ( $T_m$ ), and followed by quenching the material, which solidifies the atoms in the amorphous state as shown in Fig. 2. Switching from crystalline to amorphous state can be achieved by applying short high voltage pulse via the embedded micro-heater. Switching the PCM from amorphous to crystalline state is achieved by heating the material beyond its recrystallization temperature ( $T_c$ ), at which the growth of crystalline grains and nucleation is enabled [36], [40]. Typically as per the bias conditions reported in [42], [46], a high voltage pulse of 12 V and ( $\sim 200$  ns) is used to amorphize the material and a low voltage pulse of 7.8 V and ( $\sim 1.2 \mu s$ ) is used to crystallize the PCM. Pulse amplitude scales with the micro-fabrication process parameters of the thin-film resistor (TFR) material. The voltage required to change the GeTe states can be down scaled by reducing the resistivity of the micro-heater, either through changing the design dimensions or thickness of the thin-film. The actuation voltages can also be reduced by depositing lower resistivity crystalline material, as less device width (smaller microheater lengths, lower resistance) can be used to achieve insertion loss targets.

The RF PCM switch model in a series single-pole single-throw (SPST) configuration is shown in Fig. 4. Terminals 1 and 2 are RF input and output ports while terminals 3 and 4 are bias pads to provide actuation pulse to the switch. A simplified switch model is described in both ON and OFF state is highlighted with the ON-state represented by a series  $R_{on}$  resistor while in the OFF-state, capacitance  $C_{pc}$  dominates.

Various directly and indirectly heated GeTe based switches are reported by University of Michigan [29], [57], [60], Northrop Grumman Corp. [30], [31], [61], HRL Laboratories [32], [33], [62], [63], University of Limoges [34], and University of Waterloo [15], [19], [40], [42] are shown in Figs. 5–9, respectively. These were some of the early stage

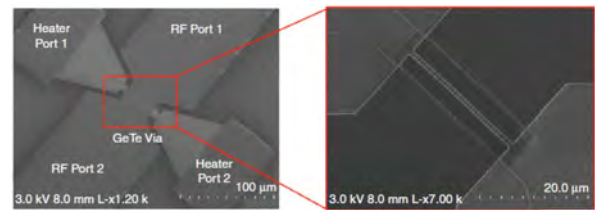


**FIGURE 5.** SEM images of GeTe based RF switch from the University of Michigan [59].

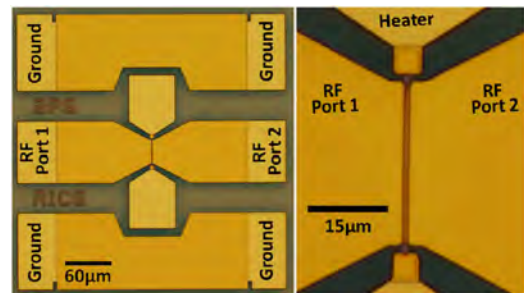


**FIGURE 6.** A low-loss phase change series RF switch from Northrop Grumman Corp. [61].

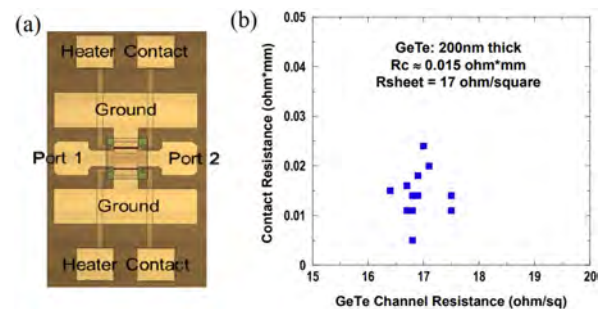


**FIGURE 7.** (a) GeTe RF switch in a shunt configuration, (b) Measured contact resistance versus GeTe channel resistance from HRL Laboratories [33].

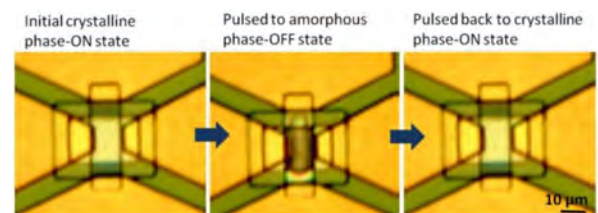


**FIGURE 8.** Optical photographs of a RF switch showing the color contrast of the GST layer in the amorphous state and in the crystalline state from the University of Limoges [34].

switches and most of these switches have a cut-off frequency of 10 THz to 12 THz with acceptable RF performance. Over the last few years, researchers from TowerSemi [47], [48], HRL Laboratories [49], [64], University of Waterloo [15], [42], [46], [65], and XLIM, University of Limoges [66] have demonstrated some state-of-the-art RF switches as shown in

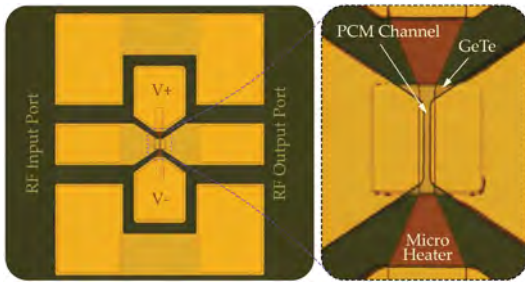


**FIGURE 9.** Optical micrograph of optimized RF PCM SPST switch from the University of Waterloo [15].

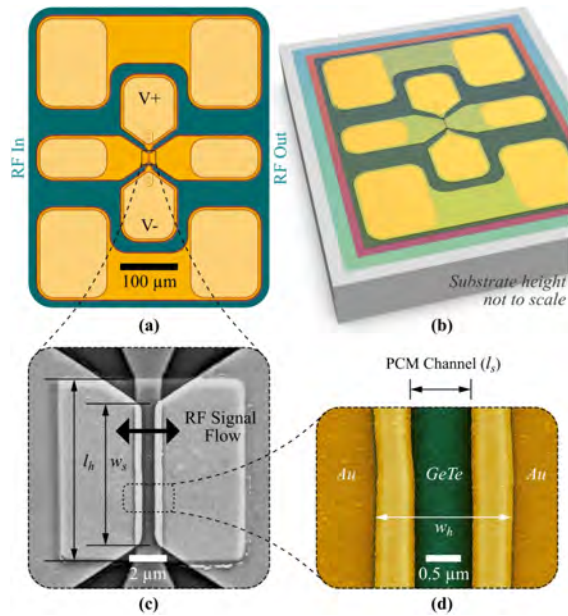


**FIGURE 10.** The University of Waterloo's PCM GeTe-based RF SPST switch. (a) Optical micrograph. (b) 3-D rendered view. (c) SEM micrograph of the switch junction showing width of the channel ( $w_s$ ) and length of the embedded microheater ( $l_h$ ). (d) False colored SEM micrograph of zoomed-in view of the PCM channel highlighting channel length ( $l_s$ ) and width of the microheater ( $w_h$ ). [42].

Figures 10 and 11 with exceptional RF performance over a wide-band.

The PCM junction dimensions are highlighted in an optical micrograph from the University of Waterloo in Fig. 10. The RF signal input and output ports and bias ports for actuation signal are shown in Fig. 10(a). The device is fully passivated and can be used for heterogeneous integration via flip-chip or by wire-bonding. A false coloured SEM image shows the closeup view of the narrow PCM channel ( $l_s$ ) and width of the micro-heater ( $w_h$ ) in Fig. 10(b). RF electrodes overlap the micro-heater to avoid switch failure due to cracks formation in GeTe near to the edges of micro-heater as discussed in [15], [67]. Fig. 10(c) and (d) depicts SEM micrographs of the junction. The overall switch area of the fabricated switch is  $400 \times 500 \mu\text{m}$ , including the test pads.

Another interesting chalcogenide PCM SbTe-based RF SPST switch is reported by HRL Laboratories [49]. Optical

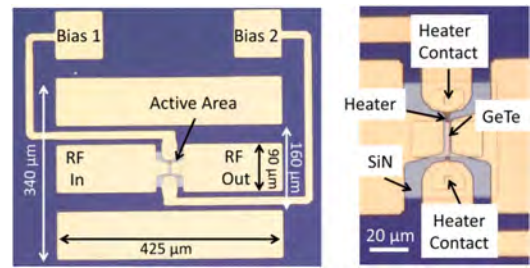


**FIGURE 11.** Optical microphotographs of PCM-based SPST CPW switch, without integrated decoupling bias circuitry from XLIM, University of Limoges [66].

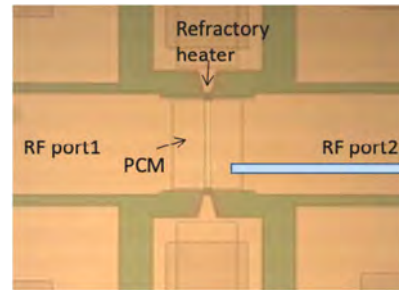


**FIGURE 12.** Optical micrograph of a SbTe based shunt RF switch from HRL Laboratories [33].

micrograph of the SbTe based RF switch is shown in Fig. 12. The switch design topology and fabrication process is similar to the previously reported RF switches except from the material composition. SbTe does not offer RF performance as comparable to that of GeTe based switches due to the higher ON state resistance and lower OFF state resistance compared to GeTe-based RF switches. The advantage of SbTe material is the lower temperature required for melt-quench sequence. The melting temperature of SbTe material depends on the material composition. Generally, SbTe melts at  $635^\circ\text{C}$ , which is approximately  $100^\circ\text{C}$  lower than GeTe melting temperature. The SbTe based switch reported in [49] claims 10 million switching cycles endurance. PCM SbTe is primarily used for memory applications, but characterization and optimization of SbTe alloy ratio might allow getting the optimal resistivity for improved RF switches in near future.

Apart from the PCM based RF single-pole single-throw (SPST) switches, various multi-port switches have been reported recently including but not limited to DC-65 GHz SPDT switch from Northrop Grumman Corp. [55] shown in Fig. 13, multiport DC-30 GHz C-type and R-type switch shown in Fig. 14, and a DC-67 GHz T-type switch shown in Fig. 15 from the University of Waterloo [38], [39], [65], [68], and TowerSemi's various DC-40 GHz SPnT switches monolithically integrated with SiGe BiCMOS process [69] as depicted in Fig. 16.

#### D. TYPICAL RF PERFORMANCE OF THE PCM SWITCH

The measured and simulated results of the fabricated PCM-based RF SPST switch from the University of Waterloo are



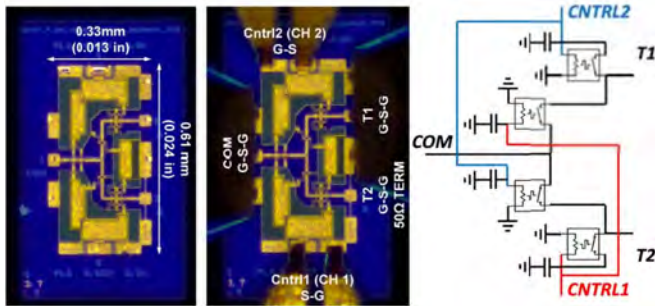


**FIGURE 13.** A PCM GeTe RF SPDT switch from Northrop Grumman Corp. [55].

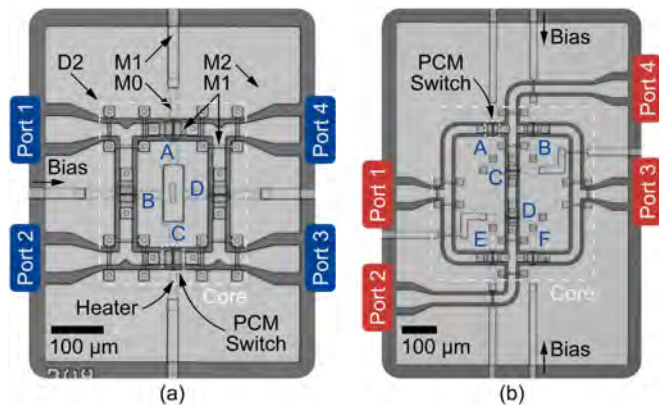


**FIGURE 14.** (a) C-type RF PCM switch. (b) R-type RF switch with additional route for routing the RF signal from the University of Waterloo [65].

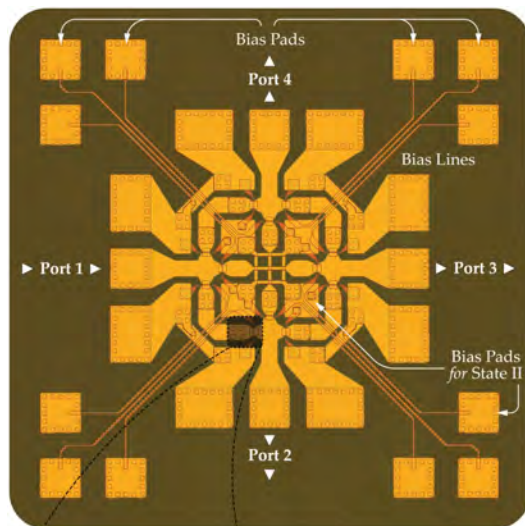


**FIGURE 15.** A DC-67 GHz T-type phase-change switch from the University of Waterloo [68].

shown in Fig. 17 [42]. It exhibits an insertion loss less than 0.4 dB up to 60 GHz. The developed switches not only compete with the state-of-the-art but also outperform in certain aspects. Insertion loss and isolation performance is measured

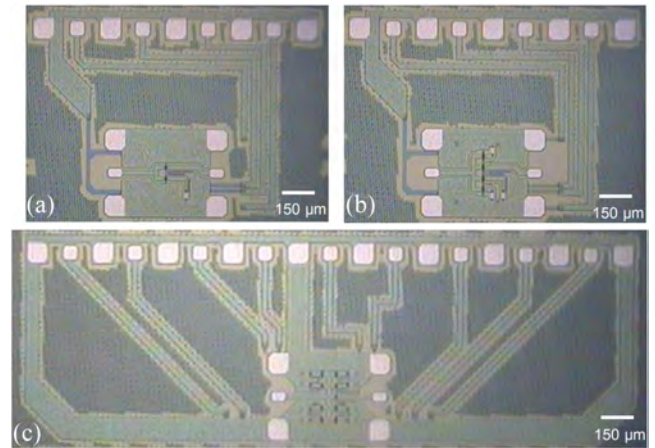


**FIGURE 16.** SPnT PCM switches monolithically integrated with SiGe BiCMOS from Tower Semiconductor [69].

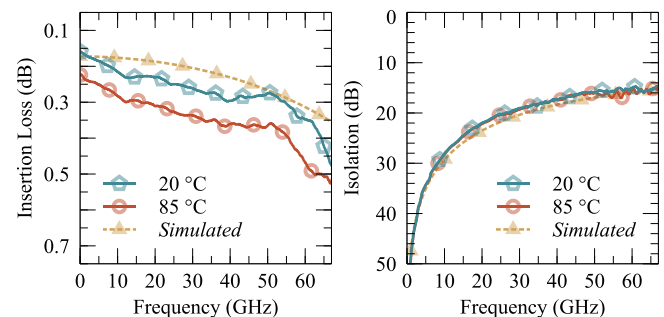


**FIGURE 17.** Measured insertion loss and isolation performance the PCM RF SPST switch over DC to 67 GHz at 20 °C and 85 °C from the University of Waterloo [42].

at 20 °C and 85 °C. An increase in insertion loss with temperature is due to the increase in resistance of the material at crystalline state. Various parameters of the switch including switch cycle testing, RF performance measurements, two-tone linearity, high-power handling, current carrying capacity, self-actuation, and reliability (lifetime cycles) have been experimentally measured and reported in [42] and show similar results to other performers.

The RF power handling of an RF switch is yet another important performance metric as it determines the maximum input power that the switch can withstand without any permanent degradation in electrical performance. For semiconductor switches, this power handling capability is affected by factors such as the number of FETs stacked in series, the control voltage applied to the FETs, and the type of diode used. The RF power handling capability of PCM switches is limited by current density in the ON-state, and voltage-breakdown in the OFF-state [39], [40], [42], [49].

## E. COMPARISON WITH STATE-OF-THE-ART

It is essential to compare the reported PCM-based switches with the current state-of-the-art. GaAs MMIC and CMOS are top of the line switches in terms of short switching time and

**TABLE 2.** Comparison With the State-of-the-Art RF Switches [42]

Technology	Device	Frequency Range (GHz)	Control Voltage (V)	Switching Time 10–90%	Insertion Loss (dB) at $f_{\max}$ *	Isolation (dB) at $f_{\max}$ *	Linearity TOI (dBm)
PCM GeTe <sup>a</sup>	SP3T	DC–67	12 V <sup>†</sup>	1.2 $\mu$ s	1.2	16	41
UltraCMOS SOI <sup>b</sup>	SP2T	DC–60	$\pm 3$ V	12 ns	2.8	136	48
GaAs MMIC <sup>c</sup>	SP2T	DC–50	–5 V	11 ns	3.0	30	40
Silicon SOI <sup>d</sup>	SP4T	DC–44	$\pm 3.3$ V	50 ns	3.0	31	50
SOI RF-MEMS <sup>e</sup>	SPST	DC–40	8 V	2 ms	2.8	14	—
GaAs pHEMT <sup>f</sup>	SP2T	DC–20	–7 V	10 ns	1.7	39	41
Magnetic Relay <sup>g</sup>	SP2T	DC–18	12 V <sup>†</sup>	7 ms	1.1	31	—
RF-MEMS <sup>h</sup>	SP4T	DC–14	3.6 V	75 $\mu$ s	3.0	10	69
RF-MEMS <sup>i</sup>	SP4T	DC–20	90 V	15 $\mu$ s	1.0	18	95
PCM GeTe <sup>j</sup>	SP2T	DC–65	6.5 V <sup>†</sup>	2 $\mu$ s	1.1	39	—
VO <sub>2</sub> <sup>k</sup>	SPST	DC–280	$\sim 2$ V <sup><math>\delta</math></sup>	—	2	13	55
PCM GeTe <sup>l</sup>	SPST	DC–67	—	—	6	19	—
PCM SbTe <sup>m</sup>	SPST	DC–50	6.5 V <sup>†</sup>	1 $\mu$ s	1	16	—
PCM-SiGe BiCMOS <sup>n</sup>	SPST	DC–67	—	—	0.6	20	42

<sup>a</sup> University of Waterloo<sup>c</sup> Analog Devices, Inc., Part No. HMC986A<sup>e</sup> University of Waterloo [6]<sup>g</sup> Teledyne Relays, Part No. GRF121<sup>i</sup> Menlo Micro, Inc., Part No. MM5130<sup>k</sup> Teledyne Scientific [72],  <sup>$\delta$</sup>  Calculated<sup>m</sup> HRL Laboratories [50]\*  $f_{\max}$  = maximum operation frequency<sup>b</sup> pSemi, Part No. PE42525<sup>d</sup> Analog Devices, Inc., Part No. ADRF5046<sup>f</sup> Analog Devices, Inc., Part No. HMC347B<sup>h</sup> Analog Devices, Inc., Part No. ADGM1304<sup>j</sup> Northrop Grumman Corp. [57]<sup>l</sup> HRL Laboratories [73]<sup>n</sup> Tower Semiconductor [74]<sup>†</sup> No steady state power consumption.

low control voltage requirements but lack in RF performance compared to other technologies. Most of the commercial RF switches are available in multi-port configurations. For a fair comparison, the RF PCM GeTe-based multi-port device is compared with the commercially available state-of-the-art multi-port RF switches developed using various technologies. The measured  $S$ -parameters of the RF switches used for comparison are taken directly from the manufacturers. The performance of various PCM single-pole three-throw (SP3T) switch [39], single-pole double-throw (SP2T) switch [55], [72], and single-pole single-throw switches [49], [71] is compared with various broadband microwave switches developed using commercial RF-MEMS, magnetic relay, GaAs pHEMT, mmWave switches developed in-house using SOI-MEMS [6], and commercial Silicon-CMOS, UltraCMOS SOI, and GaAs MMIC technologies. Part number of the compared devices are given in the footnotes of Table 2. The RF switches used in comparison in Table 2 have their performance pros and cons over the others [42].

The RF performance of the compared devices in the ON and OFF-states is shown in Fig. 18, and a comparative summary in tabular form is provided in Table 2. The RF PCM GeTe switch developed using the reported microfabrication process [42] and Northrop Grumman Corp.'s fabrication process [55], outshines other technologies with its exceptional and best-in-class insertion loss performance especially at mmWave range. It offers the smallest die size among the state-of-the-art, has non-volatile or latching functionality, and adequate switching speed.

It is worth highlighting the contribution from Teledyne Scientific [70] demonstrating MIT VO<sub>2</sub> DC-280 GHz RF switch with exceptional performance. The fundamental limitation of the VO<sub>2</sub> technology is the low transition temperature of 68 °C, which is not suitable for commercial 85 °C specifications. The VO<sub>2</sub> based switches are also not usable for high RF power applications as the heat from the RF signal could potentially reach beyond 68 °C transition point and could self actuate the switches. Due to the constant bias requirement, these switches also have a slow transition speed. However, VO<sub>2</sub> based switches are excellent candidates for various low power RF applications where the surrounding temperature won't exceed more than 50 °C and doesn't require high switching speed. The UltraCMOS SOI technology-based single-port double-throw (SPDT) switch demonstrates excellent isolation, reasonable insertion loss till 60 GHz, low voltage, but has 15 $\times$  larger chip area than the PCM GeTe SP3T switch. The TOI of the PCM GeTe reported in the comparison is measured for the SPST series switch.

Two commercially available and highly reliable single-pole four-throw (SP4T) RF-MEMS switches that guarantee more than one billion switching cycles are also included in the comparison. Currently available commercial RF-MEMS demonstrate exceptional linearity performance but only work up to 22 GHz. The compared RF-MEMS switch from Analog Devices, Inc. (Part No. ADGM1304) has power handling capability close to the PCM GeTe switches, but is much larger in size. An RF-MEMS switch from Menlo Micro, Inc. (Part No. MM5130) exhibits up to 44 dBm CW RF power handling and



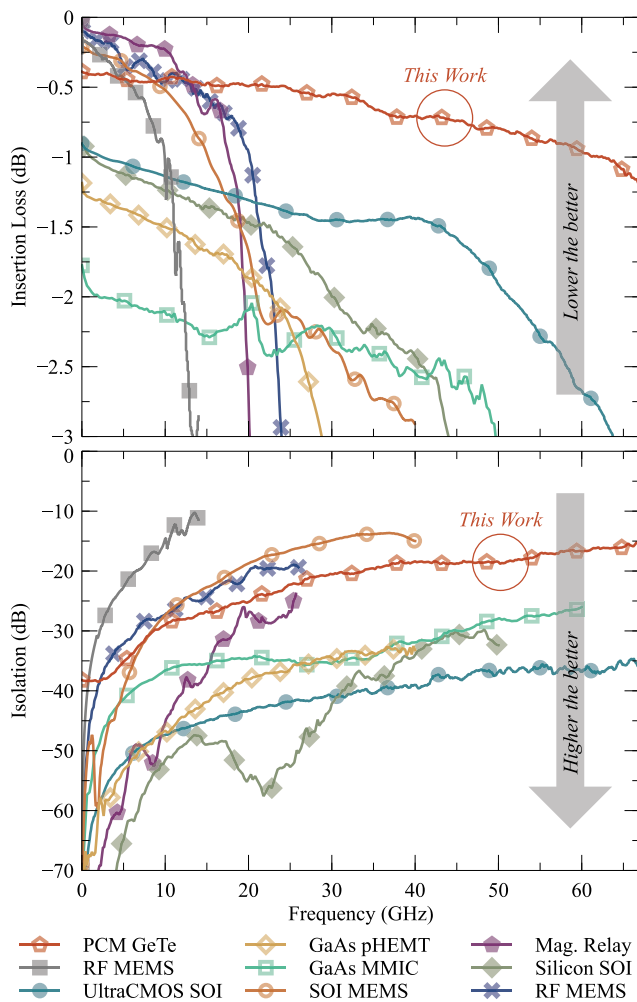


**FIGURE 18.** Measured insertion loss and isolation performance of current state-of-the-art RF switch technologies. Measured S-parameters data of the commercial RF switches are taken directly from the manufacturers [42].

exceptional IIP3 of 95 dBm, but is large in size and requires a high 90 V as a bias voltage.

The magnetic relay offers excellent RF performance, latching functionality, and outstanding power handling capability among the competition, but works up to 18 GHz only, reliable till 3 million cycles with a slow switching time of 7 ms. Magnetic relays also have a relatively much larger size.

Out of all the RF devices compared, each switch technology is unique in some way or the other and also lacks in one or more aspects. Switch technology selection choice all comes down to the applications and frequency range. It depends on the use case scenario or application to decide which performance parameter is the switches' primary selection criteria. The emerging PCM GeTe-based developed switches push the boundaries by offering a technology that leads to devices with broadband operation frequency, low insertion loss, and miniature die size [42], [49], [55], [71], [72]. Although, the PCM technology offers many advantages over other RF switch technologies, but it is worth highlighting one of the drawback

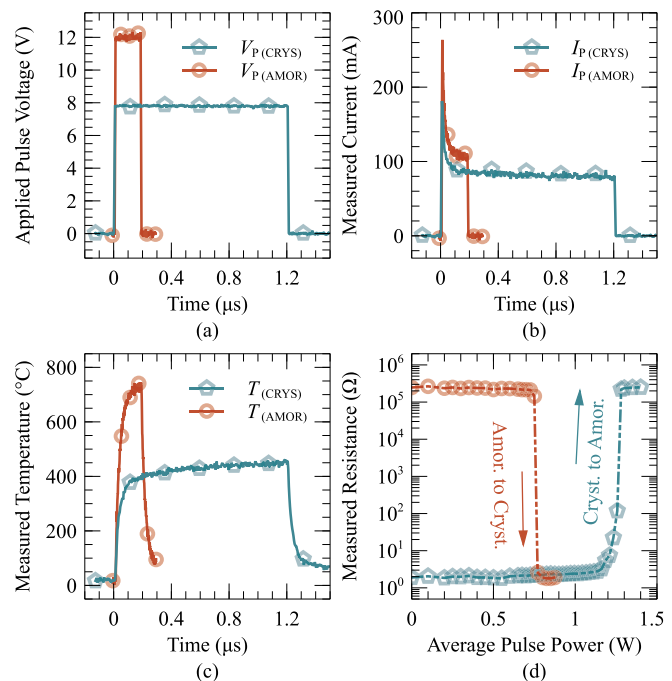


**FIGURE 19.** Control signal applied to the RF PCM GeTe-based SPST switches for achieving non-volatile/latching reversible phase change between crystalline and amorphous state. (a) Applied amorphous and crystalline voltage pulse. (b) Measured current. (c) Measured temperature. (d) Resistance of the device for applied average pulse power highlighting more than five orders of reversible resistance change [42].

of PCM switches, namely the power consumption during the transition state. While the switch is non-volatile, it does consume energy switching between states resulting in switch-rate dependent power consumption. For certain applications (such as 5G duplex T/R switch) this could result in significant power consumption compared to semiconductor technologies.

## F. BIAS SIGNATURE, RESISTANCE CHANGE AND THERMAL CROSSTALK

For biasing the monolithic RF PCM switches, example applied actuation voltage pulses are shown in Fig. 19(a) and the measured current is shown in Fig. 19(b). A high-speed tungsten micro-heater is integrated underneath the PCM GeTe with a sandwiched barrier layer. The refractory micro-heaters utilized in the fabrication process exhibit a measured linear temperature coefficient of resistance,  $\alpha$ , of  $0.0031^\circ\text{C}$  and a DC resistance of  $35\ \Omega$  at  $20^\circ\text{C}$  that is measured using a 1 mV read-out voltage. The measured temperature profile of the micro-heater is shown in Fig. 19(c). The measured resistance with varying average pulse power is shown in Fig. 19(d). The RF PCM switch described above exhibits a resistance change of over five orders of magnitude between crystalline and amorphous states. Compared to the current state-of-the-art semiconductor-based RF switches, the non-volatile functionality of the PCM GeTe switches does not consume any static DC power to hold the switch state.

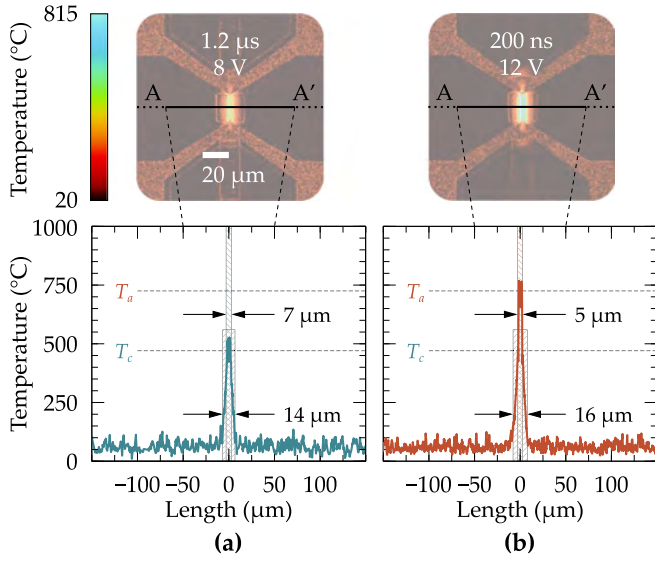


**FIGURE 20.** Heat distribution across 300  $\mu\text{m}$  A–A' cross-section of the RF PCM switch to study thermal crosstalk. (a) A crystalline pulse of amplitude 8 V and 1.2  $\mu\text{s}$  width generates sufficient heat ( $T_c$ ) to crystalline the PCM switch. (b) An amorphous pulse of amplitude 12 V and 200 ns width generates temperature ( $T_a$ ) to melt the PCM GeTe. No thermal crosstalk is seen in (a) and (b) [41].

It is worth highlighting that despite the high temperature requirements beyond 750  $^{\circ}\text{C}$ , the PCM-based RF switches can be integrated monolithically to develop complex RF devices without any thermal crosstalk concerns [19], [43]. The thermal energy is confined to the PCM junction area for few nanoseconds only. The thermal actuation crosstalk and transient heat distribution in PCM switches has been experimentally verified utilizing thermoreflectance imaging [41].

Various multi-port miniaturized monolithically integrated complex RF components require a number of switches to be integrated very close to each other. PCM technology allows very tight integration of switches due to the smaller size of switches compared to other technologies. Experimental investigation of thermal actuation crosstalk using transient thermal imaging proves no actuation crosstalk as detailed in [41]. It also provide safe limits to closely integrate PCM switches monolithically.

To investigate the thermal cross-section in PCM switches, heat profiles are measured across 300  $\mu\text{m}$  A–A' cross-section of the RF PCM switch as shown in Fig. 20 using transient thermoreflectance imaging technique.  $T_c$  is the recrystallization temperature and  $T_a$  is amorphization temperature. With a crystalline actuation pulse (8 V, 1.2  $\mu\text{s}$ ), heat distribution across the A–A' cross-section is measured at  $t=1.2 \mu\text{s}$ . No thermal crosstalk or any hot-spots are observed across 300  $\mu\text{m}$  length. Temperature rises past  $T_c$  within 7  $\mu\text{m}$  length and is less than 200  $^{\circ}\text{C}$  within 14  $\mu\text{m}$  around the junction. Metal electrodes sink the temperature, thus heat is extremely localized and confined within 15  $\mu\text{m}$  junction surface area as shown in Fig. 20(a). Amorphous pulse (12 V, 200 ns) is applied across micro-heater terminal and across A–A' cross-section,

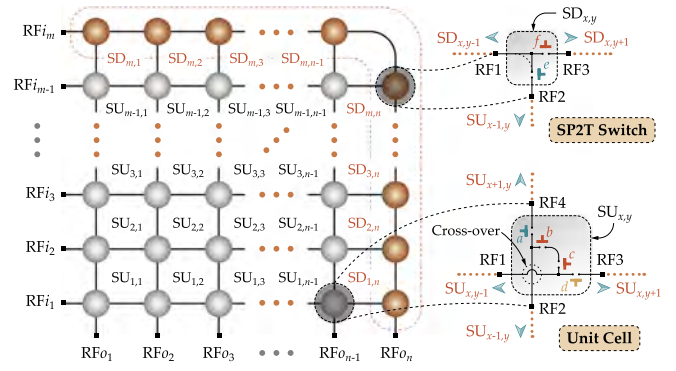


**FIGURE 21.** Scalable  $m \times n$  crossbar switch matrix architecture utilizing switch unit-cells and SP2T switches arranged in a grid pattern to achieve signal routing [46].

no thermal hot-spots or crosstalk is observed. Across 300  $\mu\text{m}$ , temperature above  $T_a$  is confined to 5  $\mu\text{m}$  junction area and is below 200  $^{\circ}\text{C}$  within 16  $\mu\text{m}$  region. With the amorphous and crystalline pulses, temperature is localized to 20  $\mu\text{m}$  area of the PCM junction and is below safe limits of 50  $^{\circ}\text{C}$  as shown in Fig. 20(b).

For the rated bias signature, RF PCM switches can be integrated as close at a distance of 20  $\mu\text{m}$ . If miniaturization is not the primary design criteria, switches should be placed at least 100  $\mu\text{m}$  apart as ultimate safe limits. Further details on the analysis is described in [39], [41]. Recently, researchers have also analytically analyzed the PCM switch models and reported the thermo-electrical design/modeling process [58], [73].

## G. PCM-BASED RECONFIGURABLE MMWAVE COMPONENTS

### 1) A SCALABLE CROSSBAR SWITCH MATRIX

Switch matrices and switching networks operating at RF and mmWave have tremendous applications in telecommunication, radar systems, and instrumentation for effective bandwidth utilization, providing efficient signal routing, and for enhancing system redundancy. A common approach towards switch matrices is to integrate several single-pole  $n$ -throw (SP $n$ T) switching unit-cells along with  $m \times n$  interconnection network. Crossbar switch matrices offer a highly miniature design and makes it easily amenable to the realization of large size switch matrices. Crossbar switch matrices typically consist of cascaded cells with signal routing functionality. In general, the crossbar switch unit cells are cascaded to form large matrices.

A scalable crossbar switch matrix architecture shown in Fig. 21 consists of an array of switch unit-cells ( $SU_{x,y}$ ) and SP2T switches ( $SD_{x,y}$ ) connected in a grid pattern to achieve signal routing. RF signal at any  $m$  input ( $RF_{i1}, RF_{i2}, \dots, RF_{im-1}, RF_{im}$ ) can be routed to any available  $n$  output port ( $RF_{o1}, RF_{o2}, \dots, RF_{on-1}, RF_{on}$ ). Cross-over paths designed in switch unit-cells offer signal routing between two overlapping RF paths. With the switch architecture shown in Fig. 21,

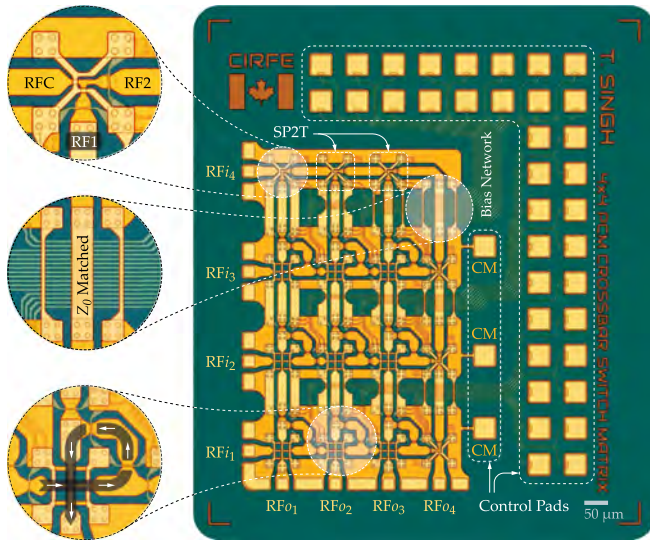


**FIGURE 22.** Optical micrograph of the PCM GeTe-based  $4 \times 4$  switch matrix. Inset shows magnified optical micrographs of SP2T switch elements, impedance matching and capacitance compensation of bias network, and a unit-cell implemented in switch matrix highlighting turn state [46].

a  $m \times n$  crossbar switch matrix requires a total of  $(mn - 1)$  total cells, with  $((m - 1) \times (n - 1))$  switch unit-cells and  $((m - 1) + (n - 1))$  SP2T switches [45], [46].

An optical micrograph of the PCM GeTe-based  $4 \times 4$  switch matrix is shown in Fig. 22. Inset shows magnified optical micrographs of SP2T switch elements, impedance matching and capacitance compensation of bias network, and a unit-cell implemented in the crossbar switch matrix highlighting turn state. The crossbar switch matrix is highly miniaturized with overall device size of  $0.5 \times 0.75 \mu\text{m}$  including RF input and output ports and excluding control pads. With the control pads arrangement depicted in Fig. 22, the device periphery is  $0.96 \times 0.77 \text{ mm}$ .

The RF performance is measured between 7 unique routes to get minimum and maximum performance limits of the  $4 \times 4$  crossbar switch matrix as shown in Fig. 23. In best case scenario (Route 1), the signal passes through two PCM SPST switches, one  $90^\circ$  bend and one RF crossover junction. While, in the worst case (Route 7), the signal is routed between  $\text{RF}_{i4}$ – $\text{RF}_{o4}$  ports, which consists of 6 SPDT switches, one  $90^\circ$  bend and three bias bridges with more than 16 conductive bias wires crossing underneath bias bridges. Despite of all the signal degradation elements in the RF path, the switch matrix is designed to exhibit less than 4.2 dB insertion loss in worst case. Most of the signal routing combinations show performance with loss less than 4 dB, measured return loss is better than 18 dB and isolation higher than 26 dB over DC to 40 GHz. EM simulated performance shows a close match with the measured results with worst case loss lower than 3.2 dB, return loss better than 20 dB and isolation higher than 26 dB. The difference between the measured and simulation insertion loss is due to the fabrication tolerances and deposited material properties different from simulation models.

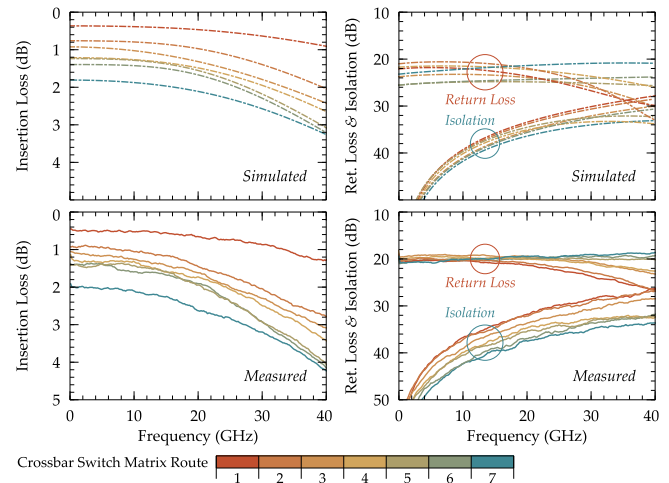


**FIGURE 23.** Measured and simulated RF performance of a PCM GeTe-based  $4 \times 4$  switch matrix over DC to 40 GHz. RF performance is shown for 7 possible routes, with route 7 exhibiting the worst case scenario [46].

## 2) MMWAVE PHASE SHIFTERS

Phase shifters are crucial components for electronic beam steering in phased-array systems. Phase shifters are widely used to change the excitation phase of an individual antenna element in phased-array antennas. mmWave phased array antennas provide the capability of real-time beam steering with high efficiency in a miniaturized package for applications including but not limited to high-speed 5G cellular communication, automotive radar and satellite communication.

A 3-bit mmWave switched true-time-delay (TTD) phase shifter based on PCM GeTe is discussed. The phase shifter is designed using four monolithically integrated PCM SP3T switches to route the signal through delay lines. The insertion loss variation between various states is minimized by integrating two fixed PCM GeTe elements maintained in the crystalline state, along with optimized width of the delay lines. The SP3T switches are connected back-to-back in two stages to provide 3-bit phase shift with  $20^\circ$  precision.

The phase shifter is designed to operate over a 8 GHz wide frequency band with a center frequency of 30 GHz. The presented phase shifter is highly miniaturized with overall device area of  $0.42 \text{ mm}^2$ . The phase shifter exhibits a measured average loss of 4.3 dB with a variation of only  $\pm 0.3 \text{ dB}$  and a return loss better than 20 dB. It provides  $180^\circ$  linear phase shift with a figure-of-merit of  $42^\circ/\text{dB}$ . The phase shifter exhibits less than 15 ps delay with 2 ps precision per state, which is lowest compared to currently available state-of-the-art MEMS-based phase shifters.

An optical micrograph of the fabricated PCM-based 3-bit switched TTD phase shifter is shown in Fig. 24, highlighting the overall device size, control pads and delay lines and loss compensation fixed PCM elements. Inset of Fig. 24 shows the optical micrograph of the close-up view of monolithically integrated PCM SP3T switches. 3D rendered SP3T switch is also shown in Fig. 24. Control pads provide the desired phase



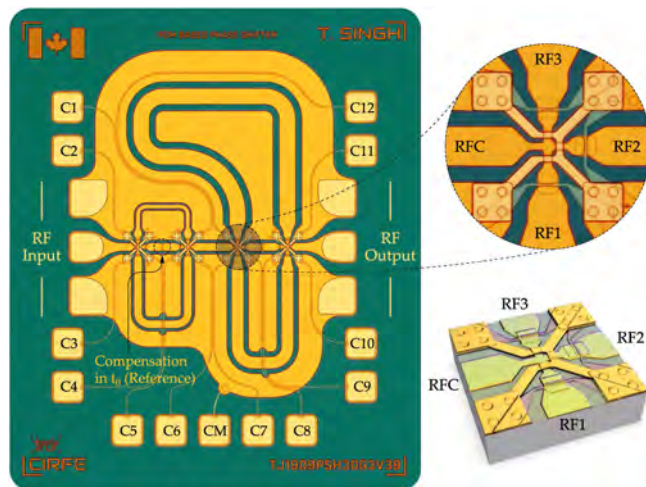


**FIGURE 24.** Optical micrograph of the monolithically integrated PCM-based 3-bit mmWave switched TTD phase shifter. Inset shows an optical micrograph of the zoomed-in view of a PCM-based SP3T switch. 3D rendered view of PCM SP3T switch core is highlighted [19].

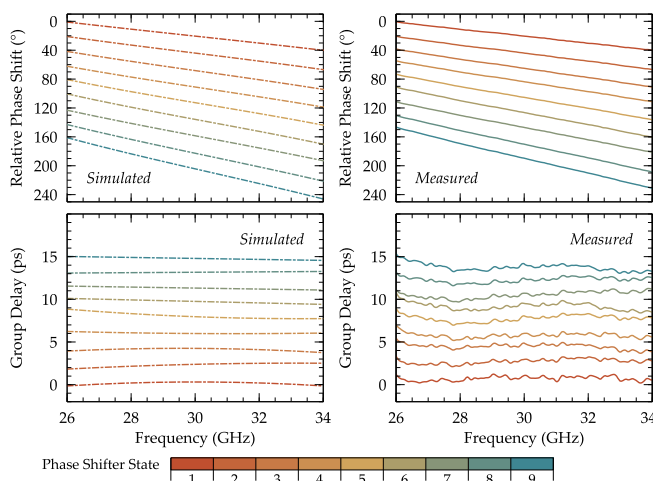


**FIGURE 25.** Measured and simulated phase shift and group delay of the PCM-based 3-bit TTD phase shifter over 26–34 GHz band. Response of all possible states is shown [19].

shift by reconfiguring the respective PCM switches in desired phase shift path. Four RF PCM GeTe-based SP3T switches (12 RF SPST switch elements) along with two fixed PCM GeTe elements  $S_0$  in  $t_0$  sections (these elements are always in the ON-state to compensate loss) are monolithically integrated to form the phase shifter as shown in Fig. 24.

Measured and simulated relative phase shift is depicted in Fig. 25 reporting highly linear  $180^\circ$  phase shift with  $20^\circ$  step precision over the operational bandwidth with figure-of-merit (FoM) of  $42^\circ/\text{dB}$ . The presented phase shifter exhibits less than 15 ps of measured group delay in 2 ps per state precision as shown in Fig. 25. The demonstrated group delay is the lowest compared to current state-of-the-art [19]. A PCM true-time-delay circuit monolithically integrated with SiGe BiCMOS is demonstrated in [74].

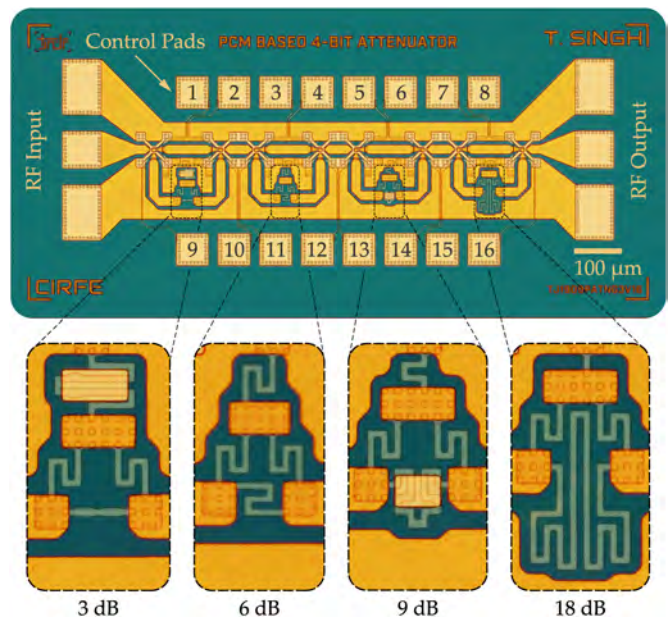


**FIGURE 26.** Optical micrograph of the monolithically integrated PCM-based 4-bit variable attenuator. Control pads 1–16 are used to tune the attenuation levels. Four passive bridged-T attenuator sections are shown in zoomed-in view [18].

### 3) WIDEBAND MMWAVE DIGITAL ATTENUATOR

Variable attenuators are commonly used for adjusting signal levels in various radio frequency (RF) circuits such as full duplex wireless systems, radar systems, automatic gain control amplifiers, vector modulators to name a few [75]. Miniaturized attenuators with high linearity and precision are highly in demand particularly for millimeter wave (mmWave) application [76]. Ka-band especially at 28 GHz have tremendous applications for 5G wireless communication systems especially beamforming networks [18].

The monolithically integrated PCM-based 4-bit attenuator from the University of Waterloo is designed by utilizing SPDT switches to route the RF signal through a section of transmission line or through an attenuator section (bit). Four attenuator bits (A–D) are cascaded to form a 4-bit device. Individual attenuator bits are designed using high frequency wide-band integrated passive bridged-T resistor networks to provide discrete attenuation levels. Bits (A–D) provides attenuation level of 3 dB, 6 dB, 9 dB and 18 dB respectively. Combining four bits provides 16 discrete attenuation levels [18]. An optical micrograph of the fabricated reconfigurable PCM-based 4-bit attenuator is shown in Fig. 26, highlighting the overall device size, control pads and individual passive bridged-T attenuators. Embedded high frequency wide-band resistors are optimized for the desired 8 GHz frequency band. Eight SPDT switches are monolithically integrated to load/unload desired passive bridged-T resistor network which provides certain attenuation in the RF path. Measured and simulated RF response of the proposed PCM-based 4-bit variable attenuator is shown in Fig. 27 from 24 GHz to 32 GHz. The response of all 16 states (4-bit) is demonstrated in Fig. 27. EM simulated

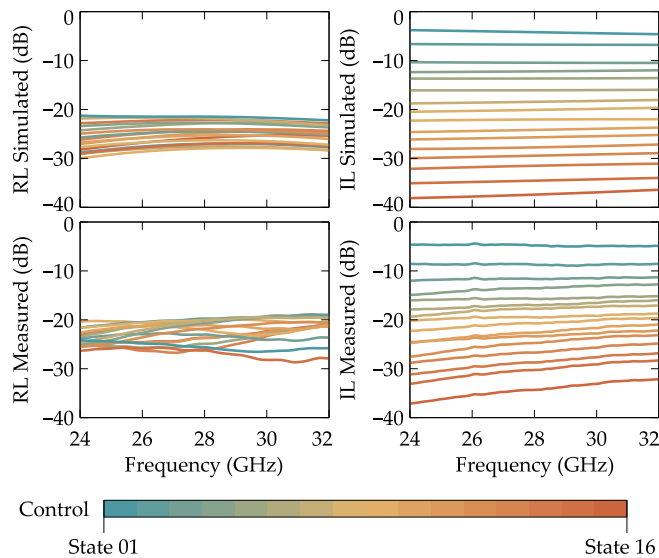


**FIGURE 27.** Measured and simulated insertion loss and return loss of the proposed PCM-based 4-bit variable attenuator over 24–32 GHz band. Response of all 16 states (4-bit) is shown [18].

response shows minimum attenuation of 3.6 dB and maximum attenuation of 38 dB at 28 GHz. All measurements were done on wafer at room temperature. Measured RF response exhibits minimum attenuation of 4.7 dB and maximum attenuation of 37 dB at the centre frequency. Simulated and measured return loss is better than 20 dB over the bandwidth. Attenuator bits (A–D) are designed to provide fixed attenuation relative to reset state, where all attenuator bits are unloaded. Another 4-bit mmWave phase change attenuator is reported by Northrop Grumman demonstrates 1, 2, 4 and 8 dB bits in [77].

## IV. OTHER POTENTIAL PCMS FOR RF APPLICATIONS

### A. OVONIC SWITCHING

Discovered in 1980 by S. Ovshinsky [78], Ovonic switching is the method many phase change materials (PCMs) go through in order to convert from amorphous to crystalline and back again. The ovonic switching method involves the formation of a conducting filament through the phase change material, changing it to the crystalline state. In order to switch back to the amorphous state, this filament must be broken or disrupted in order to interrupt the conducting pathway. This type of filamentary switching can occur in two different types of devices: ovonic threshold switching devices, where the filament is temporary, only existing as long as a bias is applied, and ovonic memory switching devices, where the filament is permanent, until a new trigger is applied to break the filament [79]. Ovonic threshold switching devices are often used as selectors, and can be useful in RF applications for things such as delay lines, due to their volatile nature. Ovonic memory switching devices are used for memory storage, but can be useful in RF applications for any RF switch that is required to hold the information until a new trigger is applied, highlighting their non-volatile nature. As shown in

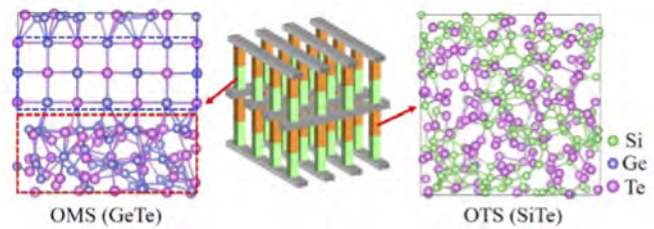


**FIGURE 28.** The key components of the 3D phase-change memory product (middle) are OMS data storage medium (left) and OTS selectors (right). The disordered configuration in the red rectangle in the left panel represents the amorphous state, while the ordered structure is the crystalline state. In contrast, the ideal OTS materials should remain amorphous without any phase transition, thus requiring high thermal stability.

Fig. 28, ovonic memory materials, such as GeTe, have two distinct states, a disordered amorphous state, and an ordered crystalline state, which can be toggled with certain triggers. Ovonic threshold materials, such as SiTe, on the other hand, remain in the amorphous state, and only form a filament when a bias is applied to the material. In general, the materials in this section present challenges for RF applications due to relatively high ON resistance and high OFF capacitance.

### B. SILICON TELLURIDE

Silicon Telluride (SiTe) is a chalcogenide material that operates as an ovonic threshold switching material, meaning the filament formed is only temporary, and therefore the switching is volatile. SiTe creates homopolar bonds (Si-Si and Te-Te) in addition to heteropolar bonds (Si-Te). This varies from other materials, such as GeTe, which exhibits primarily heteropolar bonds (Ge-Te) [79]. Variations in SiTe behavior can be seen between unannealed and annealed films (annealed under vacuum at 300°C for 30 s), but both have potential for RF applications. The following values were measured for a device area of 5  $\mu\text{m}$  by 5  $\mu\text{m}$  by 50 nm. For unannealed films, SiTe exhibits a 50 ns transition time from high resistance (230 kOhm) to low resistance (1.8 kOhm) at a threshold of 0.4 V. For annealed films, SiTe exhibits a 35 ns transition time from high resistance (1.2 MOhm) to low resistance (6.6 kOhm) at a threshold of 0.7 V. Using a memristor endurance test, SiTe devices demonstrated 100 k cycles before failure [80]. The SiTe process is also back-end-of-line compatible with the CMOS process, which is very important in considerations for modern RF switch technologies. The schematic diagrams explaining the volatile switching mechanism of threshold selectors is shown in Fig. 29.

### C. HAFNIUM OXIDE

Hafnium Oxide (HfOx) is a binary transition metal oxide which behaves in a similar way to vanadium oxides. HfOx switching is non-volatile, meaning it will retain a state until switched again. Interestingly, with proper tuning of the structure, HfOx can also operate in a volatile manner. To switch HfOx from a high resistance to a low resistance state,



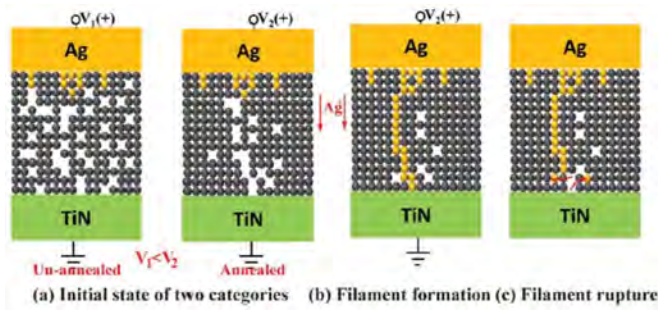


**FIGURE 29.** Schematic diagrams explaining volatile switching mechanism of threshold selectors. (a) The blank denotes the grain boundary for Ag migration. The annealing process helps the nano-crystals in as-deposited layer grow and nucleate and decrease the amounts of grain boundaries for Ag atoms migration. Thus there is much less grain boundaries in annealed devices (right) than un-annealed devices (left). (b) Ag atoms forms filimsy filament under electrical stimulus. (c) Filament spontaneously ruptures after removing voltage. [80].

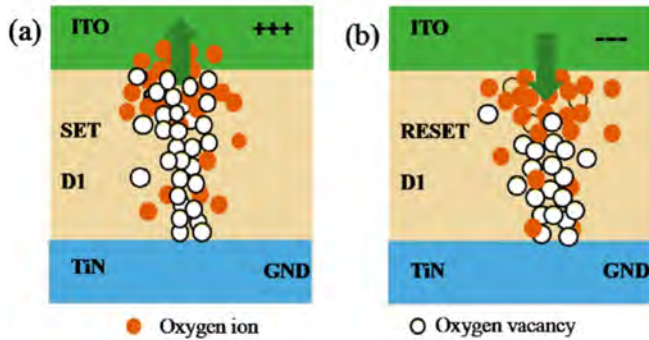


**FIGURE 30.** Schematic diagram of the switching mechanism (a) from high resistance to low resistance state and (b) from low resistance to high resistance state. The green arrow represents the movement direction of oxygen ions, the green box is the top electrode, and the blue box is the bottom electrode [81].

a positive pulse of approximately 1 V for less than 20  $\mu$ s was applied. To switch from the low resistance to the high resistance state required a negative pulse of approximately  $-1$  V for less than 25  $\mu$ s [81]. While HfOx acts like non-volatile chalcogenides, in that it holds its state, it is worth noting that the switching behavior mimics that of a memristor, requiring a positive voltage to switch one way, and a negative voltage to reverse that switching. It is thought that oxygen vacancies are attracted to the positive bias, allowing a hafnium filament to form, creating a conducting pathway through the material. When a negative voltage is applied, oxygen ions enter the HfOx film and fill the vacancies, breaking the filament, as seen in Fig. 30 [81]. It can also be found in [81], that doping the HfOx with Sulphur increases the switching speed and lowers the energy necessary to switch between states. HfOx is also one of the most established materials in the CMOS domain, making it an excellent candidate for RF applications.

#### D. ZINC TELLURIDE

Zinc Telluride (ZnTe) is a chalcogenide material that, like SiTe, demonstrates ovonic threshold switching, or volatile

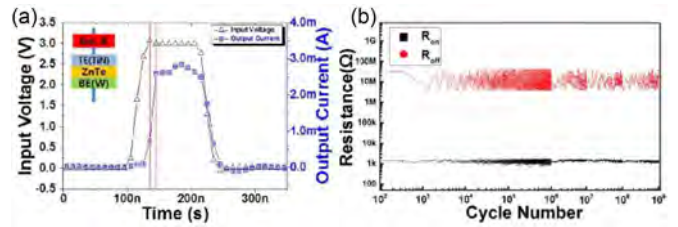


**FIGURE 31.** (a) Voltage and current characteristics for input pulse. (b) Endurance testing for threshold switching of ZnTe device, showing no significant variation over 1 billion switching cycles [82].

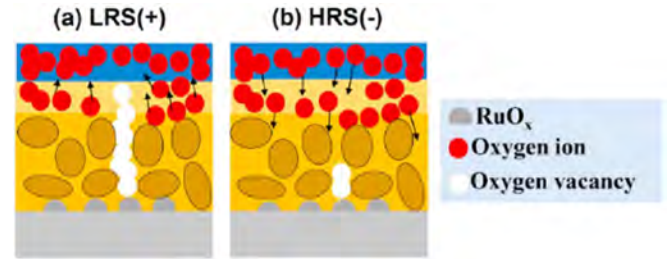


**FIGURE 32.** Schematic diagram of TaOx device under (a) positive voltage and (b) negative voltage [83].

switching behavior. ZnTe devices demonstrated in [82] were formed with a TiN/ZnTe/W metal-chalcogenide-metal stack, and were found to have a selectivity of over 10<sup>4</sup> and thermal stability over 400 °C. These ZnTe devices demonstrated extremely fast threshold switching of 10 ns, a high resistance of approx. 10 MOhm, a low resistance of around 1 kOhm, and endurance of 1 billion switching cycles. Input pulses to trigger the low resistance state were 3 V, with pulse width of 100 ns, and rise/fall time of 20 ns. Characteristics and endurance testing results can be seen in Fig. 31. ZnTe devices exhibit similar characteristics to Germanium Antimony Telluride (GST), a common chalcogenide used in commercial memory applications, but ZnTe provides a volatile switching option as compared to the non-volatile switching of GST.

#### E. TANTALUM OXIDE

Tantalum Oxide (TaOx) is a transition metal oxide material, and like HfOx, demonstrates non-volatile switching triggered by opposite polarity bias. TaOx is appealing due to easy fabrication and good reliability endurance in combination with a metastable layer [83]. TaOx devices form a conducting filament when a positive voltage is applied to the top electrode. The device remains in this state until a negative voltage is applied to the top electrode, breaking the filament as seen in Fig. 32. TaOx devices in [83] demonstrated a high resistance state of approximately 3 kOhm, a low resistance state of 3 Ohm, and an endurance of more than 10 million cycles, with some degradation of the high resistance state manifesting after  $3 \times 10^3$  cycles.



## V. HISTORY OF METAL INSULATOR TRANSITION MATERIALS

Since the discovery of MIT by F. J. Morin at Bell Labs in 1959 [84], the initial research was mainly focused on the understanding of MIT transition behavior [85]. Meanwhile, preparation of the stable forms of vanadium oxides for microelectronic devices got the attention among the researcher. In 1965, Futaki [86] was the first who reported the development of sensitive thermistors based on vanadium dioxide; the use of such thermistors in an oscillator at frequencies up to 1 MHz implies a switching speed of less than  $1\ \mu\text{s}$ . Takei and Koide in 1966 [87] reported the epitaxially grown  $\text{VO}_2$  single crystal film on substrate and observed the electrical resistivity change of  $1\ \text{k}\Omega$ . This is the same time when the study of infrared optical properties of vanadium dioxide above and below the transition temperature was performed by A. S. Barker in 1966 [88] which paved the way for electro-optical device applications. As the vanadium oxide has large number of distinct phased, initial research was dedicated towards the careful optimization of the working parameters required to obtain thin films of the pure  $\text{VO}_2$  phase.

MIT materials are a group of materials that are capable of switching between metal and insulator states through the application of external stimuli, such as mechanical (external pressure or strain), optical (photon excitation), temperature (conductive heating) and electrical stimuli (charge injection or Joule heating). There are many different materials, such as  $\text{RNiO}_3$ ,  $\text{Fe}_3\text{O}_4$ ,  $\text{BaVS}_3$ ,  $\text{Ti}_2\text{O}_3$ ,  $\text{V}_2\text{O}_3$ ,  $\text{V}_2\text{O}_5$ ,  $\text{V}_3\text{O}_5$ ,  $\text{V}_4\text{O}_7$ ,  $\text{V}_5\text{O}_9$ ,  $\text{V}_6\text{O}_{11}$ ,  $\text{V}_8\text{O}_{15}$ , and  $\text{VO}_2$  [89]. Their electrical conductivity changes abruptly at a certain temperature, which is called the transition temperature ( $T_t$ ). Among various other MIT materials, only the  $\text{VO}_2$  has  $T_t$  of  $68^\circ\text{C}$  that makes it quite suitable for many practical applications.

Cope and Penn [90] reported the first solid-state thermal switches with fast switching of 20 ns. During the recent decades the advancement in thin-film deposition using e beam evaporator [91], pulsed-laser deposition (PLD) [92] and rf sputtering provided the necessary technologies to achieve the single-phase vanadium dioxide. Later in 1991, P. J. Hood and J. F. DeNatale [91] reported the dielectric properties of epitaxial grown  $\text{VO}_2$  thin films at mm-wave frequency (at 38 GHz). This gives an insight on thickness dependent permittivity change of  $\text{VO}_2$  thin films that are strongly influenced by microstructure, crystalline orientation, grain-boundary stress, and stoichiometry at mm-wave frequency.

## VI. METAL INSULATOR TRANSITION IN VANADIUM DIOXIDE ( $\text{VO}_2$ )

Vanadium dioxide ( $\text{VO}_2$ ) has attracted tremendous attention among the researchers owing to its lower MIT transition at  $68^\circ\text{C}$ . Although the most common method to induce the phase change in  $\text{VO}_2$  material is through temperature (conductive heating), other triggering mechanism such as electrical (charge injection of Joule heating), optical (photon excitation) and mechanical (pressure or strain) are also well documented. An activation time as short as 100 fs has been

reported for the optically driven MIT transition [93], and the electronically induced transition occurs within nanoseconds [94], which paved the way towards various exciting application. Since the optical absorption and electrical resistance changes,  $\text{VO}_2$  has shown as a emerging material candidate for electrical switching [94], optical switching [95], thermochromic smart windows [96], sensor [97], terahertz [98], memories [99], and field-effect [100]. In addition, drastic changes in its resistivity and permittivity during MIT transition led  $\text{VO}_2$  to be considered for many RF microwave applications.

E. Sovero et al. [101] performed the first RF characterization of  $\text{VO}_2$  switches followed by Michael Stotz et al. [102] and F. Dumas-Bouchiat et al. [92], a key contributors towards the investigation of  $\text{VO}_2$  based RF switching performance. After several reports on  $\text{VO}_2$  based RF switches, the pioneering work on using  $\text{VO}_2$  switches for tunable filter and reconfigurable antenna was initiated by Julien Givernaud et al. [103] and Dimitris E. Anagnostou et al. [104], respectively.

A thermally driven RF switch using the properties of metal insulator transition in  $\text{VO}_2$  was reported by XLIM in 2010 [105] and Harvard University in 2013 [106]. Teledyne reported a high performance RF switch based on MIT materials in 2015 [107]. The switch reported shows promising results for millimeter wave frequencies till 50 GHz with cut-off frequency of 45 THz. The heating mechanism is implemented using integrated chip heaters to provide local thermal control. The switch reported 0.13 dB of insertion loss and 20 dB isolation till 50 GHz. Dynamic range for this switch is  $(4.4 \times 10^4)$  with low resistance of  $3.3\ \Omega$  at  $68^\circ\text{C}$ .

In the last decade, there was tremendous interest in tunable and reconfigurable  $\text{VO}_2$  based microwave components including but not limited to phase-shifter [108], absorber [109], inductor [110], actuator [111], attenuator [112], reflectarrays [113] and intelligent reflective surface (IRS) [114]. Recently, A. Shamim [115], [116], [117], [118], [119] has come with an idea of printing  $\text{VO}_2$  switches, which paved a way for additively manufactured reconfigurable RF components.

### A. PRINCIPLE OF OPERATION

The MIT in  $\text{VO}_2$  takes place at around  $68^\circ\text{C}$ , accompanying the lattice structural transition from a high-temperature rutile structure (R phase) to a low-temperature monoclinic structure (M phase) and vice versa, as illustrated in Fig. 33. The monoclinic structure (M phase) corresponds to an insulator or semiconductor characteristic due to V-V zigzag chains in its crystal structure (a). However, when the temperature is above ( $T_t$ ), the  $\text{VO}_2$  adopts a rutile structure (R phase), which corresponds to a metallic characteristic due to linear arrangement of V-V atoms (b). In addition to electrical characteristics,  $\text{VO}_2$  also shows selective infrared (IR) switching. For example, at low temperature monoclinic phase, it allows infrared to transmit while at high temperature rutile phase the IR is blocked. It is worth mentioning that there is still no model about the MIT that can explain broad range of phenomenon

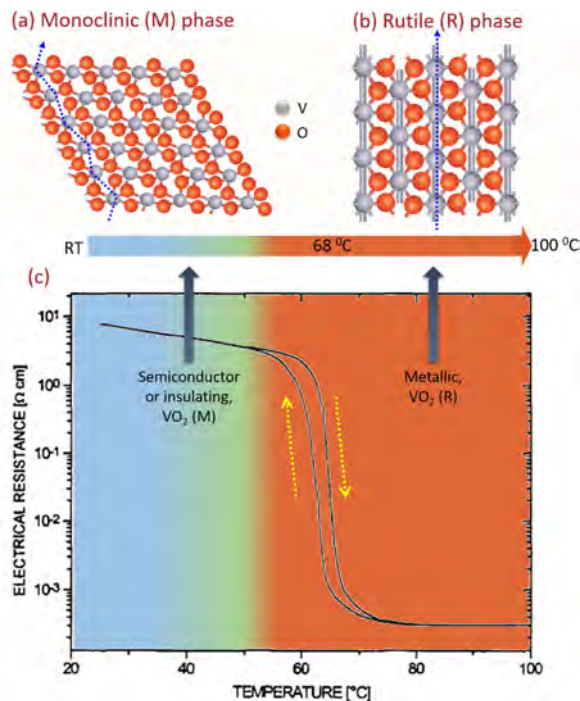


**FIGURE 33.** The VO<sub>2</sub> in (a) monoclinic, (b) rutile crystal structures and (c) Temperature dependence of the resistivity based on the fully-reversible phase transition [102].

occurring in the material. The precise mechanism of the MIT in VO<sub>2</sub> is long been disputed among temperature driven mechanism arising from instabilities in electron-lattice dynamics (Peierls-like transition) and a pure electronic mechanism due to strong electron-electron correlations (Mott-MIT transition) or the cooperation of both mechanisms. The MIT induces an electrical resistance of VO<sub>2</sub> changes by 3-5 order of magnitude depending on the crystalline quality of deposited films, elemental stoichiometry and doping. For example, VO<sub>2</sub> films produced in a plasma assisted reactive evaporation process demonstrated reversible resistivity change of  $10^4 \Omega\text{-cm}$  with the hysteresis width of  $3^\circ\text{C}$  (as shown in Fig. 33(c)) [102]. The change in state of VO<sub>2</sub> from metal into an insulator and vice versa makes it quite attractive for electrical engineering applications.

## B. RF SWITCHES

Compared to other MIT materials, VO<sub>2</sub> appears to be suited to practical RF-switching applications because of its lower MIT temperature ( $68^\circ\text{C}$ ). Thus, it has drawn attention from researchers interested in this domain and there have been several demonstrations of VO<sub>2</sub>-based RF switches in last three decades. For example, E. Sovero et al. [101] reported the first microwave switch, employing VO<sub>2</sub> thin films, consisting of a microstrip transmission line on a GaAs substrate compatible with IC technology. They observed insertion loss of less than 1 dB in the ON state and more than 12 dB in the OFF state at 40 GHz with fast response time of 30 ns (ns). Later, Michael Stotz et al. [102] reported the thermally controlled

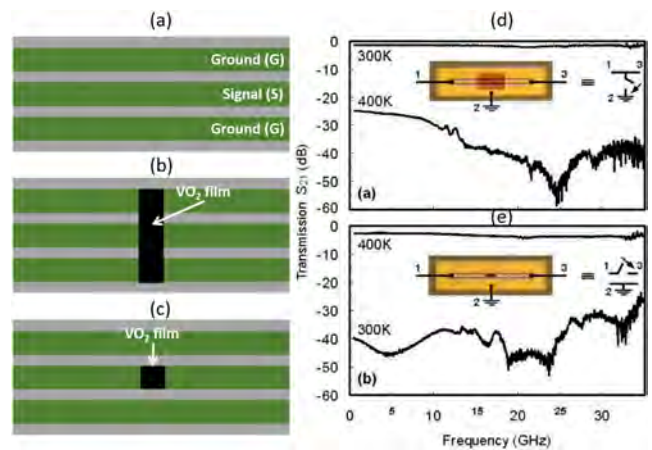


**FIGURE 34.** Illustration of (a) CPW transmission line, (b) shunt switch, and (c) series switch. The measured  $S_{21}$  parameters of (d) VO<sub>2</sub> shunt RF switches and (e) VO<sub>2</sub> series RF switches [92].

novel coplanar VO<sub>2</sub> switches designed for 24 GHz operation on sapphire substrate. VO<sub>2</sub>-films was produced in a plasma assisted evaporation process, which demonstrated smaller resistivity change ( $1 \text{ k}\Omega$  to  $10 \text{ k}\Omega$ ) as compared to VO<sub>2</sub> single crystal (105). The single pole single throw (SPST) and single pole double throw (SPDT) devices have shown the insertion loss of 2.7 dB and 2 dB at ON state, with isolation of -25 dB and -18 dB at OFF state, respectively. Later on, F. Dumas-Bouchiat et al. [92] reported pulsed-laser deposited (PLD) VO<sub>2</sub>-thin films switches on Al<sub>2</sub>O<sub>3</sub> substrate using shunt and series configuration with coplanar waveguide (CPW) lines, as shown in Fig. 34. For the shunt switch, VO<sub>2</sub> is deposited such that it covers an entire part of the CPW line that includes the signal and the ground traces (Fig. 34(b)). It operates in the following way: at room temperature (or zero excitation current), VO<sub>2</sub> film is not conducting, so it allows the RF signal to pass through the metallic signal trace (this is termed the ON condition for the switch). When the VO<sub>2</sub> film is activated, either through thermal or current excitation, it becomes conductive and thus shorts the signal trace to the ground traces. Therefore, nothing is transmitted through the CPW line (this is termed the OFF state of the switch). In the case of the series switch configuration, in contrast to the shunt switch configuration, as shown in Fig. 34(c), at room temperature (or zero current excitation) VO<sub>2</sub> film is not conducting, thus the gap in the signal trace does not allow any signal transmission (OFF state).

When the VO<sub>2</sub> film is activated, it becomes conductive and thus bridges the gap at the signal trace, allowing signal transmission (ON state). In the shunt configuration, low losses of 0.8 dB is observed at OFF state and with ON state the attenuation of 25 dB until 12 GHz, and higher than 35 dB from 13 to 35 GHz is observed (as shown in Fig. 34(d)). In the series configuration, average attenuation of 40 dB is observed at OFF state while 2.5 dB insertion loss when the switch is turned ON (Fig. 34(e)). With such VO<sub>2</sub> switch performance, further

research dedicated to explore the failure behavior and reliability test for their integration in practical electronic circuits. For example, A. Crunteanu et al. [120] performed systematic lifetime investigations of 10 GHz series configuration based VO<sub>2</sub> switches activated by voltage and current-controlled modes. They observed more than 260 million and almost 16 million cycles without failure when activated through current and voltage, respectively. Thus, the lifetime was at least 16 times longer for the current-driven than the voltage-driven VO<sub>2</sub> devices, primarily; due to current-induced activation is less affected by thermal effects, resulting in a smaller degradation of the VO<sub>2</sub> films. As the fabrication techniques advances, J. Leroy et al. [121] reported the high speed switching of 4.5 ns with 125 nm gaps between two electrodes that was achieved using optical lithography and shadow evaporation. Sieu D. Ha et al. [106] reported a VO<sub>2</sub> switch that had 25 dB of isolation and 3 dB of IL, up to 13.5 GHz. This switch was fabricated using nanofabrication methods and utilizing RF sputtering (at 550 °C). The same group [122] also observed that increasing input RF power lowers the insertion loss of VO<sub>2</sub> similarly as increasing bias current which was in good agreement with the delivered power for a voltage-driven phase transition, demonstrating that RF power alone can trigger the phase transition of VO<sub>2</sub>. C. Hillman et al. [123] reported a SPST based VO<sub>2</sub> switch, which have the lowest insertion losses of 0.2 dB at 50 GHz with isolation of 21.5 dB and 0.5 dB at 110 GHz with isolation of 15 dB. The same group also expanded the frequency range to 220 GHz with insertion loss of 1.3 dB and isolation of 15.7 dB. These switches have been fabricated having an off-state capacitance of approximately 4 fF and ON state resistance of about 1 Ohm. Such switches reached a 40 THz cut-off frequency with low power budget (2 V, 8 mA) enabling high-performance millimeter wave devices.

As noted in the above, each type of conventionally fabricated VO<sub>2</sub> based RF switch has both advantages and disadvantages. It is realized that the cost of reported VO<sub>2</sub> switches is understandably high due to the involvement of complex and expensive nanofabrication processes. In addition, these switches are not flexible because of the rigid substrates used in their implementation. To reduce the fabrication cost and render RF switches compatible with wearable and conformal applications, additive manufacturing is an attractive option. Thus, printed VO<sub>2</sub> based switches are attractive and only a few tiny layers at the site of interest will be suffix to control the device functionality. In this regard, Vaseem et al. [115] developed VO<sub>2</sub> nanoparticles based electronic ink which was later on used for the fully inkjet-printed switches by Shuai et al. [117]. The authors proposed CPW based shunt and series configuration. It was observed that the printed VO<sub>2</sub> film has limited conductivity under both the activated and non-activated conditions. The conductivity in combination with the size of the VO<sub>2</sub> switch determines the resistance of the VO<sub>2</sub> switch, which directly affects its RF performance.

The simulation for both types of RF switches with different resistance is illustrated in Fig. 35. For the series configuration shown in Fig. 35(a), the IL decreases with the decreased

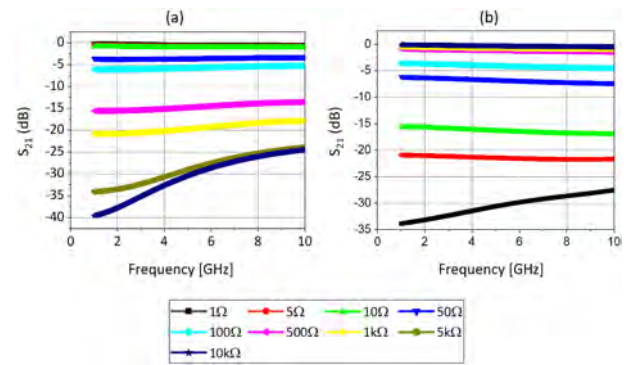


**FIGURE 35. Simulated  $S_{21}$  of the RF switches with different resistance. (a) Series switch. (b) Shunt switch.**

resistance. Inversely, for the shunt configuration shown in Fig. 35(b), the IL increases as the resistance decreases. The conductivity of the inkjet-printed VO<sub>2</sub> film is tested in the range from about 4 S/m to about 620 S/m under non-activated and activated conditions, respectively. Therefore, the resistance ratio is estimated at 150. Considering this value and observing Fig. 35(a), it is concluded that a possible resistance combination is 10 Ohm and 1.5 kOhm for the series configuration, which offers a balanced RF performance in terms of IL and isolation. Similarly, in the case of the shunt configuration shown in Fig. 35(b), a possible resistance combination is 5 Ohm and 750 Ohm. However, it is worth noting that the ideal resistance combination is dependent on different applications, where the isolation is more important than the IL, or vice versa. The inkjet-printed VO<sub>2</sub> switches demonstrates that the ratio of the resistance between non-activated and activated conditions is in the range of 120 and 180, which is comparable to some other VO<sub>2</sub> switches [92]. These switches have shown good performance from very low frequencies up to 40 GHz. In the OFF state, isolation ranging from 30 to 15 dB have been achieved (from low to high frequency, respectively). In the ON state, insertion loss of around 1 dB has been achieved for shunt configuration and around 3 dB for the series configuration. A more than 100 ON/OFF ratio and a switching speed of 0.4  $\mu$ s have been achieved.

Later on, the same group realized that to improve the electrical performance from inkjet-printed devices, thick films (tens of micrometers) are typically required; thus, tens or hundreds of printing passes are necessary to generate high-quality VO<sub>2</sub> films, which is not favorable for high-efficiency fabrication, especially for large-area printing. Thus, Weiwei Li et al. [119] reported the preparation of high-crystalline VO<sub>2</sub> microparticles and report a simple route to produce VO<sub>2</sub> ink suitable for screen-printing techniques [119]. With this ink, authors demonstrated high-throughput printing of VO<sub>2</sub> switches on both flexible polymers (Kapton and poly [ethylene terephthalate] (PET)) and rigid sapphire wafers with high resolution (down to 60  $\mu$ m) at high speed over a large area. The screen-printed VO<sub>2</sub> switches exhibited excellent electrical performance with ON/OFF ratio of 300, as shown



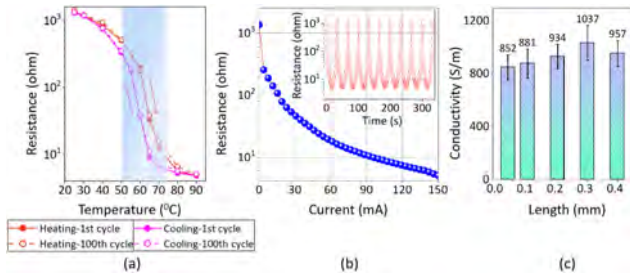


**FIGURE 36.** (a) The measured resistance of the screen-printed VO<sub>2</sub> switch at different temperatures in the heating and cooling process. (b) The measured resistance at different bias currents of 10 nA and 150 mA. (c) The calculated electrical conductivity as a function of switch length. Inset in (b) is showing the resistance as a function of cyclic electrical triggering [119].

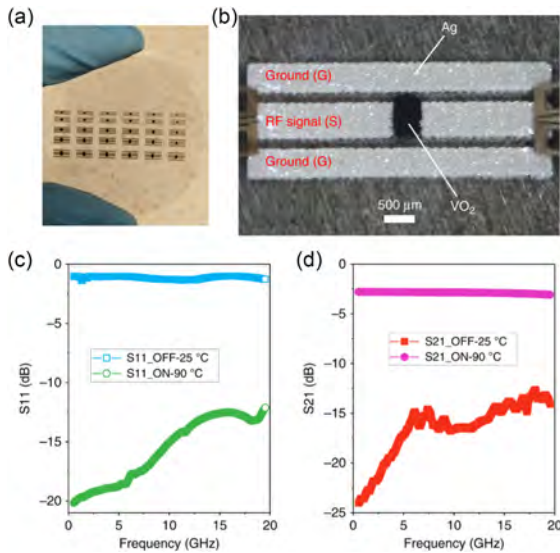


**FIGURE 37.** (a) Digital photograph of the fully screen-printed series switches on a sapphire wafer. (b) Optical image of one series switch under the RF performance test. (c) The measured  $S_{11}$  of the series switch at 24 °C and 90 °C. (d) The measured  $S_{21}$  of the series switch at 24 °C and 90 °C [119].

in Fig. 36(a). A similar resistance response was observed by applying different bias currents to the VO<sub>2</sub> switches, as presented in Fig. 36(b). One important exception with the electrical stimulus is the maximum current applied to the switch. It is observed in the measurements that a 160 mA of current can permanently damage the switch and render it usefulness. Thus, for this case the current should be increased step by step. The conductivity values in the ON state for all the samples are almost similar with some minor fluctuations (in the range of 852 to 1037 S/m) (Fig. 36(c)). These values are superior to the value of 180 S/m obtained for inkjet-printed VO<sub>2</sub> films [117] primarily due to high crystalline microparticles used in screen-printing ink.

After DC characterization, authors have screen-printed the CPW lines with VO<sub>2</sub> on sapphire substrate, as shown in Fig. 37(a) and (b). The measured  $S_{11}$  for screen-printed series switches, at room temperature (OFF state), resulted -1 dB over the entire measured frequency range up to 20 GHz, as shown

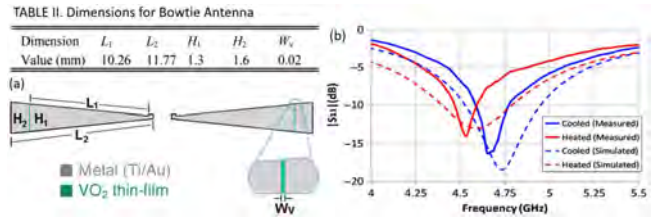


**FIGURE 38.** (a) The layout of a reconfigurable bowtie antenna with VO<sub>2</sub> (turquoise) on both arms [124]. (b) The simulated and measured  $S_{11}$  for the heated (up to 90 °C) and cooled (to 21 °C) bowtie configurations [124].

in Fig. 37(c). This was also confirmed by the  $S_{21}$  measurement, in which less than -13 dB was observed (Fig. 37(d)). In contrast,  $S_{11}$  became lower than -12 dB, and  $S_{21}$  increased to -2.6 dB IL when the temperature was 90 °C, demonstrating a reasonable transmission of the RF signal.

### C. RECONFIGURABLE ANTENNAS

An interesting component which helps in achieving reconfigurability is RF switch. Thus, the VO<sub>2</sub> switches are used in multiple reconfigurable antenna design. For instance, Dimitris E. Anagnostou et al. [124] reported the first proof-of-concept bowtie antenna design working around 4.5 GHz using VO<sub>2</sub> as the catalyst (VO<sub>2</sub> thin film deposition using PLD) for reconfigurability (Fig. 38(a)). The bowtie antenna was fabricated on a sapphire substrate that is fed using a coaxial sleeve balun. The fabricated antenna shifts its frequency when VO<sub>2</sub> is thermally heated, as shown in Fig. 38(b). At room-temperature (when VO<sub>2</sub> is not heated), the measured antenna gain was 0.14 dBi while heated state resulted -0.67 dBi. They expected that the reduced antenna gain with heated state was primarily due to losses attributed by the series capacitance of thin and narrow VO<sub>2</sub> film with adjacent thicker metal arms of the antenna which resulted power being stored within the antenna near field. Authors suggested that the series capacitance can be minimized by depositing a thick and larger VO<sub>2</sub> but with the cost of slower switch. Although, the antenna has lower efficiency of 40.7% when heated and 48.9% when cooled, the results proven that VO<sub>2</sub> can be used in the creation of reconfigurable antennas. In addition, It should be noted that the VO<sub>2</sub> on the antenna was activated using an external directive heating source which is much slower than the electrical activation. Later on, L. Huitema et al. [125] reported the frequency reconfigurability using VO<sub>2</sub> with electrical activation that was explored for millimeter wave frequency domain. Initially, the authors design and fabricated a VO<sub>2</sub> switch based CPW line to extract the VO<sub>2</sub> dielectric properties, as shown in Table III, Fig. 39.

Once the VO<sub>2</sub> materials properties were extracted, it has been integrated within antenna device designed for optimizing its response up to 40 GHz. The antenna design was based on a slot radiating element excited with a microstrip line (50 Ohm) having a length that can be varied with VO<sub>2</sub> switch, as shown in Fig. 39(a). The microstrip line feeds the millimeter-waves to the device, and is also used to apply the DC-bias to switch

TABLE III. VO<sub>2</sub> layer properties on the (10–40 GHz)

	ON-state (no DC bias)	ON-state (electrical excitation of 2V)	ON-state (temperature excitation at 90 °C)
Conductivity (S/m)	10	$1 \times 10^5$	$3.2 \times 10^5$
Permittivity	500	10000	10000

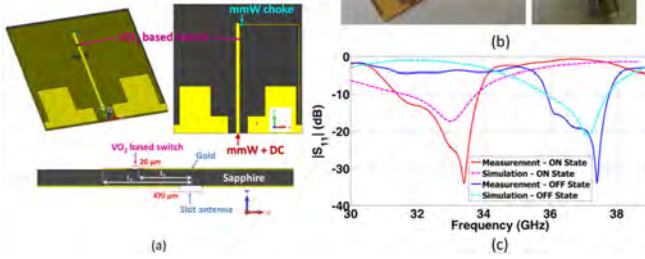


**FIGURE 39.** (a) Electromagnetic simulated design. (b) Fabricated prototype of the reconfigurable antenna. (c) The corresponding  $S_{11}$  parameters with the VO<sub>2</sub> pattern in the OFF- or ON-states [125].

the VO<sub>2</sub> film. The fabricated prototype is shown in Fig. 39(b). The ON state is obtained when applying a DC-bias voltage of 2 V at VO<sub>2</sub> terminals using mm-wave choke. Thus, depending on the VO<sub>2</sub> material state, the antenna device can be switched between 33 and 37 GHz operating frequency bands, as shown in Fig. 39(c). The frequency ratio was about 1:1.13 and maximum gains of 5.28 dBi and 5.41 dBi, respectively. The measured total efficiency was extrapolated by gain pattern integration, and the obtained values are equal to 83.5% for the ON-state case and 86% for the OFF-state.

Another notable work combined a VO<sub>2</sub>-based reconfigurable antenna platform with individually controlled micro-heater pixels capable of creating different antenna patterns with unique resonance properties [126]. In this approach, electrical stimuli was only applied to microheaters (Ni-Cr based) which transfer the heat generated to the VO<sub>2</sub> layer. Thus, authors shown a planar antenna placed on a  $9 \times 9$  micro-heater matrix that can be configured into different patterns with the operating frequencies in S-band (2–4 GHz), C-band (4–8 GHz), and X-band (8–12 GHz) which cover the entire UWB spectrum (3.1–10.6 GHz). In recent years, a variety of tunable omnidirectional circularly polarized (CP) antenna have been reported using VO<sub>2</sub>. For example, Guo-Biao Liu et al. [127] reported dual band and wideband omnidirectional CP antenna which shown a 10-dB impedance bandwidth of 45.7% (1.67–2.66 GHz) and a 3-dB AR bandwidth of 40% (1.9–2.85 GHz), when the VO<sub>2</sub> was thermally elevated at 50 °C (state I). When  $T = 80$  °C (State II), the omnidirectional CP antenna operates at a lower frequency band, with a 10-dB impedance bandwidth of 13.8% (1.62–1.86 GHz), and a 3-dB AR bandwidth of 21.8% (1.68–2.09 GHz). The same group also reported [128] another CP antenna design where at  $T \geq 68$  °C (state I), the proposed antenna has a 10-dB impedance bandwidth of 15.9% (2.09–2.45 GHz), and a 3 dB AR bandwidth of 23.4% (2.04–2.58 GHz). When  $T < 68$  °C (state II), it has a bandwidth of 6.5% (2.38–2.54 GHz) with  $S_{11}$  below –10 dB, and a bandwidth of 19.9% (2.39–2.92 GHz) with AR below 3 dB.

The proposed omnidirectional CP antenna has the advantages of wideband, reconfigurable operating bandwidth, and

temperature tailored, which is suitable for wireless communication occasions where antennas have different performance requirements. It can be observed that most of the reported VO<sub>2</sub> based reconfigurable antenna only focused on small dipole or slot antennas with relatively small frequency reconfigurable ratios and gains. In addition, mostly tuned with integrated thermal heaters or directive heating source, which is slower than the electrical activation of VO<sub>2</sub>. To overcome these shortcomings, Wanchen Yang et al. [129] reported a novel millimeter-wave frequency reconfigurable metasurface antenna (FRMSA) by electrically controlled VO<sub>2</sub> film. In brief, the VO<sub>2</sub> film was inserted into a uniplanar compact photonic-bandgap (UC-PBG) structure to achieve a frequency reconfigurable metasurfaces (FRMS). Due to convenient connectivity of the UC-PBG, a simple DC bias coplanar with the metasurfaces structure was designed. They observed that resistance of the VO<sub>2</sub> film (larger resistance at OFF state require higher bias voltage) has big influence on the bias voltage of the phase transition, the resonance, and loss of the UC-PBG after the phase transition. They realized that the resistivity reduction of the VO<sub>2</sub> film is difficult in material fabrication, thus, authors introduced interdigitated structures in UC-PBG structure to further reduce the resistances of the film in OFF and ON state. When the VO<sub>2</sub> film is at insulating state, the proposed antenna can operate in 23.25–24.3 GHz with the maximum gain of 8.7 dBi. However, by applying DC signals it can work in 37–39.8 GHz with a peak gain of 7.6 dBi when driven to metallic state. The proposed antenna exhibited larger frequency ratio and higher gain in mm-wave bands, as compared to other reported VO<sub>2</sub> based antennas, thus authors speculated that such antenna design might find potential applications in future 5G mm-wave communications systems. It is also worth highlighting a significant contribution from D. Anagnostou et al. [104], [130] highlighting the on-wafer integration of resistive heaters with the VO<sub>2</sub> antenna having DC bias lines electrically disconnected from the RF device. This significantly reduces the RC time constant and thus reducing the switching time and opens new design capabilities, mass production, and technology commercialization.

The printed VO<sub>2</sub> switches are also used in multiple printed reconfigurable antenna design on hard (glass) and soft substrate (Kapton) [50], [69], [70], [71]. For instance, Su et al. shown first a fully inkjet-printed reconfigurable PIFA antenna using VO<sub>2</sub> switches which is also assessed for its flexibility on antenna performance [50], [69]. The antenna is designed on 50  $\mu$ m thick Kapton substrate ( $\epsilon = 3$ ,  $\sigma = 0.003$  at 1 GHz) that is fed by 50 Ohm coplanar waveguide line. The VO<sub>2</sub> layer is inkjet printed in the gap of the arm of the antenna, which resulted in ‘ON’ and ‘OFF’ resistance of 10 Ohm and 1 kOhm respectively. The measured impedance performance of the antenna shows matched conditions in the frequency band of 1.7–2.5 GHz when the switch is at ‘ON’ state, while in the OFF state of the switch the antenna works from 2.75 to 3.5 GHz. The  $S_{11}$  of the antenna with different bending condition, such as convex and concave, is shown in Fig. 40(a) and (b). In case of concave bending, a maximum shift of 10 MHz



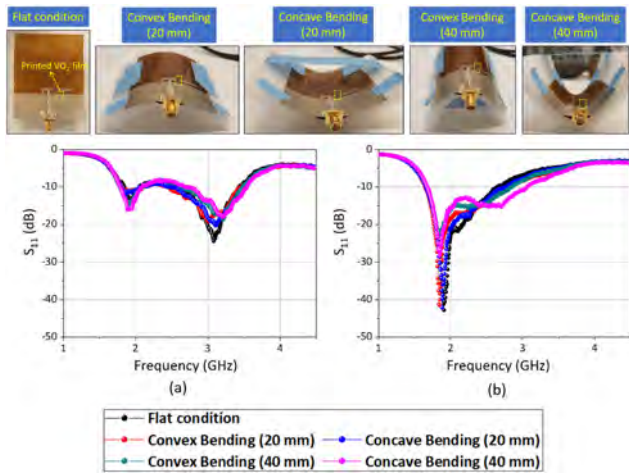


**FIGURE 40.** Flexibility assessment of PIFA antenna with different switching state (a) OFF state, (b) ON state [116].

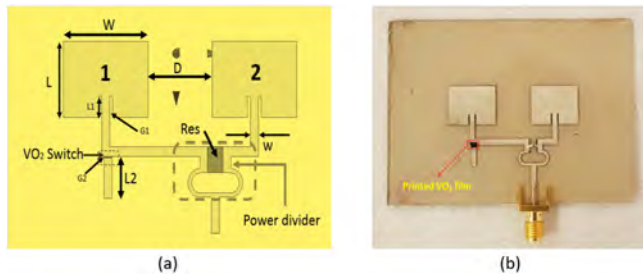


**FIGURE 41.** (a) The geometry of radiation pattern reconfigurable antenna array. (b) Fabricated prototype [131].

is observed when the switch is at OFF state and 10–40 MHz in ON state. The wide impedance bandwidth of the antenna retains the matching at the desired operating frequencies with different bending condition, which further confirms its mode of operation on flexible substrates.

In [131], radiation pattern reconfigurable antenna design has also been reported where the design comprises a power divider (with 100 Ohm resistor) to split the power into two parts and feed two patch antenna elements as labelled 1 and 2 in Fig. 41(a). In order to control the feed of the left side antenna 1, a quarter wavelength open stub ( $L_2$ ) is connected with  $\text{VO}_2$  switch. The switch with ‘ON’ state short circuited at point G2, thus no signal receive to antenna 1 from main feedline which resulted radiation only with antenna 2 with bore-sight maximum radiation pattern, as shown in Fig. 42(a). Here, the antenna array has 3 dB broad beam at the broadside from  $-56.9^\circ$  to  $54.57^\circ$  in the H-plane. In contrast, switch with ‘OFF’ state isolate the open stub from feeding line of patch antenna 1 which resulted both antenna in operation. The 3 dB beam split into two beams, one is from  $-47.75^\circ$  to  $-30^\circ$  and the other is from  $12.85^\circ$  to  $58.31^\circ$  while there is a null at boresight due to the intended phase shift between both the patch antenna elements, as shown in Fig. 42(b). The gain difference between the ‘ON’ and ‘OFF’ state is more than 13 dBs in simulation and more than 8 dBs in measurement, as shown in Fig. 42(c).

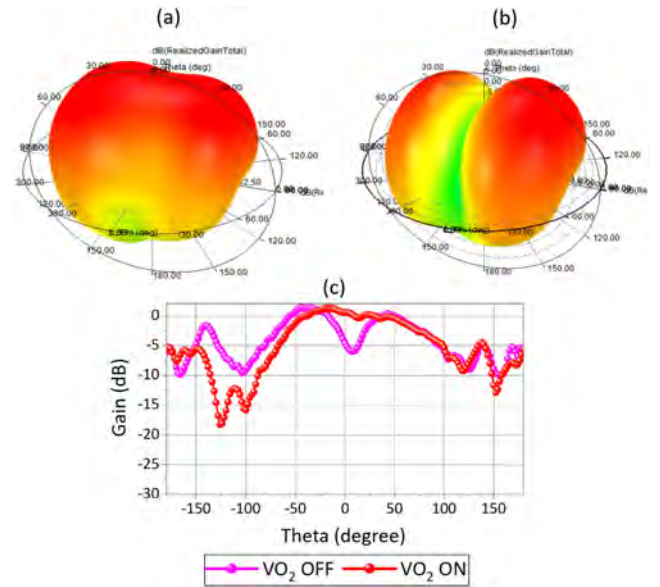


**FIGURE 42.** The radiation pattern for (a) ON state, (b) OFF state, and (c) measured gain at 5.2 GHz [131].

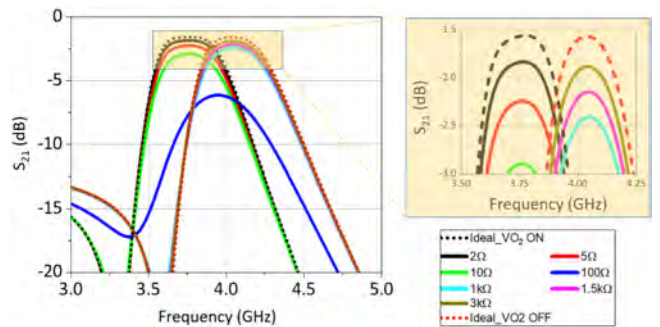


**FIGURE 43.** The simulated  $S_{21}$  of the filter while sweeping the resistance of the  $\text{VO}_2$  switch. The inset is the zoomed-in figure. (from [118]).

The results confirmed the viability of fully printed  $\text{VO}_2$  switch based radiation pattern reconfigurability.

#### D. RECONFIGURABLE FILTERS

A RF filter is an essential component in wireless systems due to their ability to control the spectral profile of the transmitter and receiver while excluding undesirable narrowband signals. In particular, bandpass filters are used to transmit the RF signal at a specific frequency band of interest, with minimal losses, while attenuating the signals as much as possible for other frequency bands. The first  $\text{VO}_2$  based tunable band stop filters operating in 11–13 GHz was reported by Julien Givernaud et al. [103]. The design consisted of transmission lines coupled with four U-shaped resonators which was fabricated in a clean room environment using classical micro fabrication technology. With the thermally and electrically activated  $\text{VO}_2$  switches integration, they proposed two types of tunable band-stop filters such as a ‘switchable stop band filter’ for which the rejection band can be switched ON and OFF and



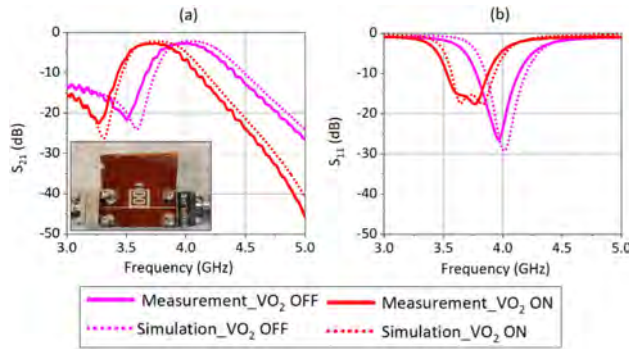


**FIGURE 44.** The simulated and measured S-parameters (a)  $S_{21}$  and (b)  $S_{11}$  of the filter at both ON and OFF states. Inset in (b) is showing the fabricated filter. (from [118]).

a “discrete tunable stop-band filter” for which the width and position of the stop-band can be discretely tuned.

Later, Wolfgang A. Vitale et al. [132] realized that high parasitic capacitance between metal contacts limited the frequency range (11–13 GHz), as reported in [103]. To overcome this problem, they introduced novel  $\text{VO}_2$ -based tunable capacitors for the design and fabrication of CMOS-compatible thermally actuated tunable bandstop filters working in the K band. The proposed device shown 12% tunability from 22.5 GHz to 19.8 GHz and insertion loss better than -2 dB up to 40 GHz. Later, Varittha Sanphuang et al. [132] reported the reconfigurable filters in terahertz (THz) domain using standard photolithography, thin-film deposition and lift-off techniques. The filters were made of frequency selective surfaces (FSS) and heater were integrated for  $\text{VO}_2$  excitation. A broadband ON/OFF filter at 0.35 THz is demonstrated with 20 dB change in transmission between the ON and OFF states. Then, a reconfigurable stopband FSS filter with tunable rejection from 0.75 to 0.55 THz was reported.

Emanuele Andrea Casu et al. [133] proposed and validates a new principle in coplanar waveguide (CPW) bandstop filter tuning by defected ground plane (DGS) design by shortcutting the turns of spiral inductor by using  $\text{VO}_2$  tuning switch. Thus, the resonant frequency was controlled by the DGS inductor self resonance. The filter was designed to work in Ka band with tunable central frequencies ranging from 28.2 GHz to 35 GHz. The measured results show a tuning range of more than 19%, a low insertion loss in the neighbouring frequency bands (below 2 dB at 20 GHz and 40 GHz in ON/OFF-states) while a maximum rejection level close to 18 dB in OFF-state. Fig. 43 and 44 illustrates the simulated and measured  $\text{VO}_2$  based tunable filter operating over 3–5 GHz band developed by Yang et al. [118].

## VII. FUTURE DIRECTIONS

Both PCM GeTe and MIT  $\text{VO}_2$  exhibit promising properties for RF applications in terms of low loss, high switching speed and good isolation performance over a broad frequency range compared to conventional semiconductor or MEMS switches. These devices also have much higher cut-off frequency and linearity compared to solid state switches. Low

cost, simple fabrication and easy integration with standard CMOS processes make these materials very appealing to the RF community.

Based on the recent advancements in the PCM and MIT materials, there are pros and cons of these materials depending on the use case scenario. PCM GeTe has certain advantages over MIT  $\text{VO}_2$  including but not limited to non-volatile operation, minimum two order of higher resistance ratio compared to MIT materials, ease in deposition, low intertion loss, high isolation, no thermal crosstalk, and reliability to name a few, makes it, an ideal material of choice for the development of reconfigurable RF devices and systems. However, the switching time is still a concern for fast tuning of various mmWave devices such as phased arrays. Various other possible PCMs such as GST, SbTe, SiTe,  $\text{HfO}_2$ , ZnTe, and TaOx are potential candidates to improve the performance of the devices. For faster switching, GST ratios can be tweaked to reduce the switching time towards ns regime, but at an expense of a high insertion loss. Extensive research from materials engineering is required to develop a PCM to have the advantages of GeTe [50:50] with high switching speed, high power handling capability and reliability. GeTe based devices also requires ultra high speed refractory micro-heater to generate high speed thermal pulses under every switching element.

On the other hand, MIT  $\text{VO}_2$  based RF devices are volatile and thus require constant bias with much lower heat requirement for actuation. Currently, the power handling capability of  $\text{VO}_2$ -based RF devices is very poor due to the lower transition temperature of 68 °C. High RF powers or high surrounding temperatures make  $\text{VO}_2$ -based devices unusable. The transition temperature can be improved by doping the material or by tweaking the V and O ratio or by doping [134]. Switching time of these devices are also worse than PCM GeTe-based devices which is one of the stringent requirement of future communication devices. From the fabrication standpoint, the MIT  $\text{VO}_2$  material can either be deposited using PLD or by molecular beam epitaxy. Both of these techniques requires a dedicated chamber and is not suitable for production foundries. The deposition of  $\text{VO}_2$  is very inconsistent due to the requirement of reactive sputtering. As depositing thin films of  $\text{VO}_2$  requires precise amount of oxygen in the sputtering chamber, slight variation of oxygen rate or pressure can produce different undesired oxides like vanadium trioxide ( $\text{V}_2\text{O}_3$ ), vanadium pentoxide ( $\text{V}_2\text{O}_5$ ) or other oxides, which do not exhibit metal-insulator transition (MIT) or in simple words, do not show resistance change behavior. Moreover, sputtering targets get oxidized fast and needs cleaning after 3–4 depositions. On the other hand, GeTe target can be used for DC sputtering. As there is no any reactive component involved, thus design to development time is short.

Printed MIT material is one possible development trajectory to lower the cost of fabrication but at an expense of low resistance ratio than the films deposited using PLD. Although a complete study of the printed  $\text{VO}_2$  switch for reconfigurable RF applications has been conducted and promising results have been achieved, the performance can be further enhanced. First, the  $\text{VO}_2$  switch has demonstrated

a maximum ON/OFF ratio of around 300. This ON/OFF ratio value is acceptable for the RF applications as presented in this paper with careful optimization steps to achieve decent results. However, higher ON/OFF ratio can not only improve the performance of the switch but also the performance of the reconfigurable components which utilize these switches. The improvement of the ON/OFF ratio is largely related to the physical properties of the VO<sub>2</sub> ink, which has to be tackled in the initial VO<sub>2</sub> nanoparticles/microparticles synthesis stage. This requires more work on chemical experiments and material characterization. Second, a trend of RF performance degradation can be observed for the VO<sub>2</sub> switch at the frequency around 40 GHz. It is expected that the performance of the switch for higher frequency ranges may further degrade, until it becomes unusable. Further development could be done to enhance the frequency of operation of the switch.

## VIII. CONCLUSION

RF switches are the fundamental building blocks for realizing reconfigurable devices in communication systems. While semiconductor RF switches are widely used in majority of commercial applications, they perform adequately up to a few GHz. The PCM and MIT-based RF devices carry the potential to realize RF switches with a superior performance up to mmWave frequencies. The PCM GeTe based switches in particular offers a unique latching capability reducing the DC power consumption. The key advantage of the PCM and MIT technologies is that it is easily amenable to monolithic integration with RF circuits such as phase shifters, tunable filters, antenna impedance tuners, switched attenuator and tunable delay lines. While recent advancements in the PCM and MIT for RF applications are promising towards the development of a wide range reconfigurable mmWave circuits, the RF PCM/MIT technology is still considered at its infancy. While there are some potential and promising materials that can be used for RF applications, but more research efforts are certainly needed to improve the switch reliability, switching speed and power handling capability to demonstrate devices for future communications.

## REFERENCES

- [1] F.-X. Pitschi and G. Spinner, "Coaxial RF switch matrix," U.S. Patent 4 829 271, May 9, 1989.
- [2] S. M. Sze and K. K. Ng, *Physics of Semiconductor Devices*. Hoboken, NJ, USA: Wiley, 2006.
- [3] B. Razavi, "CMOS technology characterization for analog and RF design," *IEEE J. Solid-State Circuits*, vol. 34, no. 3, pp. 268–276, Mar. 1999.
- [4] T. Singh, N. K. Khaira, and R. R. Mansour, "Thermally actuated SOI RF MEMS-based fully integrated passive reflective-type analog phase shifter for mmWave applications," *IEEE Trans. Microw. Theory Techn.*, vol. 69, no. 1, pp. 119–131, Jan. 2021.
- [5] M. Daneshmand and R. R. Mansour, "RF MEMS satellite switch matrices," *IEEE Microw. Mag.*, vol. 12, no. 5, pp. 92–109, Aug. 2011.
- [6] N. K. Khaira, T. Singh, and R. R. Mansour, "Monolithically integrated RF MEMS-based variable attenuator for millimeter-wave applications," *IEEE Trans. Microw. Theory Techn.*, vol. 67, no. 8, pp. 3251–3259, Aug. 2019.
- [7] R. Stefanini et al., "Miniature MEMS switches for RF applications," *J. Microelectromech. Syst.*, vol. 20, no. 6, pp. 1324–1335, 2011.
- [8] Analog Devices, Inc., "0 Hz/DC to 14 GHz, single-pole four-throw MEMS switch with integrated driver," ADGM1304 datasheet, Rev. G., Feb. 2021.
- [9] Menlo Microsystems, Inc., "MM5130 - DC to 26 GHz high power RF switch," MM5130 datasheet, Ver. 2.1, May 2021.
- [10] S. K. Bahl and K. L. Chopra, "Amorphous versus crystalline GeTe films. III. Electrical properties and band structure," *J. Appl. Phys.*, vol. 41, no. 5, pp. 2196–2212, Apr. 1970.
- [11] S. K. Bahl and K. L. Chopra, "Amorphous versus crystalline GeTe films. II. Optical properties," *J. Appl. Phys.*, vol. 40, no. 12, pp. 4940–4947, Nov. 1969.
- [12] S. R. Ovshinsky, "Reversible electrical switching phenomena in disordered structures," *Phys. Rev. Lett.*, vol. 21, no. 20, pp. 1450–1453, Nov. 1968.
- [13] M. Nardone et al., "Electrical conduction in chalcogenide glasses of phase change memory," *J. Appl. Phys.*, vol. 112, no. 7, Oct. 2012, Art. no. 071101.
- [14] A. Crunteanu, A. Mennai, C. Guines, D. Passerieux, and P. Blondy, "Out-of-plane and inline RF switches based on Ge<sub>2</sub>Sb<sub>2</sub>Te<sub>5</sub> phase-change material," in *Proc. IEEE MTT-S Int. Microw. Symp.*, Tampa, FL, USA, 2014, pp. 1–4.
- [15] T. Singh and R. R. Mansour, "Characterization, optimization and fabrication of phase change material germanium telluride based miniaturized DC–67 GHz RF switches," *IEEE Trans. Microw. Theory Techn.*, vol. 67, no. 8, pp. 3237–3250, Aug. 2019.
- [16] L. D. L. Cruz, A. G. Birdwell, M. Zaghloul, and T. G. Ivanov, "GeTe phase change research at the US army research laboratory," in *Proc. IEEE MTT-S Int. Microw. Symp.*, Philadelphia, PA, USA, 2018, pp. 843–845.
- [17] T. Singh and R. R. Mansour, "A miniaturized monolithic PCM based scalable four-port RF switch unit-cell," in *Proc. 49th Eur. Microw. Conf.*, Paris, France, 2019, pp. 180–183.
- [18] T. Singh and R. R. Mansour, "Miniaturized reconfigurable 28 GHz PCM-based 4-bit latching variable attenuator for 5G mmWave applications," in *Proc. IEEE MTT-S Int. Microw. Symp.*, Los Angeles, CA, USA, 2020, pp. 53–56.
- [19] T. Singh and R. R. Mansour, "Loss compensated PCM GeTe-based wideband 3-bit switched true-time-delay phase shifters for mmWave phased arrays," *IEEE Trans. Microw. Theory Techn.*, vol. 68, no. 9, pp. 3745–3755, Sep. 2020.
- [20] A. T. Waterman, "XXI. On the positive ionization from certain hot salts, together with some observations on the electrical properties of molybdenite at high temperatures," *Philos. Mag. J. Sci.*, vol. 33, no. 195, pp. 225–247, 1917.
- [21] S. Raoux and M. E. Wuttig, *Phase Change Materials: Science and Applications*. New York, NY, USA: Springer, 2010.
- [22] R. Neale, D. Nelson, and G. E. Moore, "Nonvolatile and reprogrammable, the read-mostly memory is here," *Electronics*, vol. 43, no. 20, pp. 56–60, 1970.
- [23] R. Shanks and C. Davis, "A 1024-bit nonvolatile 15 ns bipolar read-write memory," in *Proc. IEEE Int. Solid-State Circuits Conf. Tech. Papers*, 1978, vol. 21, pp. 112–113.
- [24] A. V. Kolobov et al., "Understanding the phase-change mechanism of rewritable optical media," *Nature Mater.*, vol. 3, no. 10, pp. 703–708, 2004.
- [25] T. Ohta, "Phase-change optical memory promotes the DVD optical disk," *J. Optoelectron. Adv. Mater.*, vol. 3, no. 3, pp. 609–626, 2001.
- [26] K. Tanaka, "Photo-induced metastability in amorphous semiconductors," *J. Non-Crystalline Solids*, vol. 37, pp. 1–10, 1991.
- [27] E. K. Chua et al., "Low resistance, high dynamic range reconfigurable phase change switch for radio frequency applications," *Appl. Phys. Lett.*, vol. 97, no. 18, pp. 95–98, 2010.
- [28] C.-Y. Wen et al., "A phase-change via-reconfigurable on-chip inductor," in *Proc. Int. Electron Devices Meeting*, 2010, pp. 10.3.1–10.3.4.
- [29] M. Wang and M. Rais-Zadeh, "Directly heated four-terminal phase change switches," in *IEEE MTT-S Int. Microw. Symp. Dig.*, Tampa, FL, USA, 2014, pp. 1–4.
- [30] N. El-Hinnawy et al., "A four-terminal, inline, chalcogenide phase-change RF switch using an independent resistive heater for thermal actuation," *IEEE Electron Device Lett.*, vol. 34, no. 10, pp. 1313–1315, Oct. 2013.
- [31] N. El-Hinnawy et al., "12.5 THz fco GeTe inline phase-change switch technology for reconfigurable RF and switching applications," in *Proc. IEEE Compound Semicond. Integr. Circuit Symp.*, La Jolla, CA, USA, 2014, pp. 1–3.

- [32] J.-S. Moon, "Method to make RF-PCM switches and circuits with phase-change materials," U.S. Patent 8900 930, Dec. 2, 2014.
- [33] J.-S. Moon et al., "10.6 THz figure-of-merit phase-change RF switches with embedded micro-heater," in *Proc. 15th IEEE Top. Meeting Silicon Monolithic Integr. Circuits RF Syst.*, San Diego, CA, USA, 2015, pp. 73–75.
- [34] A. Mennai et al., "Bistable RF switches using Ge<sub>2</sub>Sb<sub>2</sub>Te<sub>5</sub> phase change material," in *Proc. Eur. Microw. Conf.*, London, U.K., Oct. 2015, pp. 945–947.
- [35] J. Jiang, K. W. Wong, and R. R. Mansour, "A VO<sub>2</sub>-based 30GHz variable attenuator," in *IEEE MTT-S Int. Microw. Symp. Dig.*, Honolulu, HI, USA, 2017, pp. 911–913.
- [36] T. Singh and R. R. Mansour, "Chalcogenide phase change material GeTe based inline RF SPST series and shunt switches," in *Proc. IEEE MTT-S Int. Microw. Workshop Ser. Adv. Mater. Processes RF THz Appl.*, Ann Arbor, MI, USA, 2018, pp. 1–3.
- [37] T. Singh and R. R. Mansour, "Characterization of phase change material germanium telluride for RF switches," in *Proc. 48th Eur. Microw. Conf.*, Madrid, Spain, 2018, pp. 475–478.
- [38] T. Singh and R. R. Mansour, "Miniaturized DC–60GHz RF PCM GeTe-based monolithically integrated redundancy switch matrix using T-Type switching unit cells," *IEEE Trans. Microw. Theory Techn.*, vol. 67, no. 12, pp. 5181–5190, Dec. 2019.
- [39] T. Singh, "Monolithically integrated phase change material GeTe-based RF components for millimeter wave applications," Ph.D. dissertation, Dept. Elect. Comput. Eng., Univ. Waterloo, Waterloo, ON, Canada, Apr. 2020.
- [40] T. Singh and R. R. Mansour, "Investigation into self actuation limitation and current carrying capacity of chalcogenide phase change GeTe-based RF switches," *IEEE Trans. Electron Devices*, vol. 67, no. 12, pp. 5717–5722, Dec. 2020.
- [41] T. Singh and R. R. Mansour, "Experimental investigation of thermal actuation crosstalk in phase-change RF switches using transient thermoreflectance imaging," *IEEE Trans. Electron Devices*, vol. 68, no. 7, pp. 3537–3544, Jul. 2021.
- [42] T. Singh and R. R. Mansour, "Experimental investigation of performance, reliability, and cycle endurance of nonvolatile DC–67GHz phase-change RF switches," *IEEE Trans. Microw. Theory Techn.*, vol. 69, no. 11, pp. 4697–4710, Nov. 2021.
- [43] T. Singh and R. R. Mansour, "Scalable mmWave non-volatile phase change GeTe-based compact monolithically integrated wideband digital switched attenuator," *IEEE Trans. Electron Devices*, vol. 68, no. 5, pp. 2306–2312, May 2021.
- [44] T. Singh and R. R. Mansour, "Reconfigurable PCM GeTe-based latching 6-bit digital switched capacitor bank," in *Proc. 50th Eur. Microw. Conf.*, Utrecht, The Netherlands, 2021, pp. 93–96.
- [45] T. Singh and R. R. Mansour, "Scalable non-volatile chalcogenide phase change GeTe-based monolithically integrated mmWave crossbar switch matrix," in *Proc. IEEE MTT-S Int. Microw. Symp.*, Atlanta, GA, USA, 2021, pp. 420–423.
- [46] T. Singh and R. R. Mansour, "Ultra-compact phase-change GeTe-based scalable mmWave latching crossbar switch matrices," *IEEE Trans. Microw. Theory Techn.*, vol. 70, no. 1, pp. 938–949, Jan. 2022.
- [47] G. Slovin, N. El-Hinnawy, C. Masse, J. Rose, and D. Howard, "Monolithic integration of phase-change RF switches in a production SiGe BiCMOS process with RF circuit demonstrations," in *Proc. IEEE/MTT-S Int. Microw. Symp.*, 2020, pp. 57–60.
- [48] G. Slovin, N. El-Hinnawy, K. Moen, and D. Howard, "Phase-change material RF switches and monolithic integration in 180 nm RF-SOI CMOS processes," in *Proc. IEEE Int. Electron Devices Meeting*, 2021, pp. 4.4.1–4.4.4.
- [49] J.-S. Moon, H.-C. Seo, K.-A. Son, K. Lee, D. Zehnder, and H. Tai, "5 THz figure-of-merit reliable phase-change RF switches for millimeter-wave applications," in *Proc. IEEE MTT-S Int. Microw. Symp.*, Philadelphia, PA, USA, 2018, pp. 836–838.
- [50] N. El-Hinnawy, G. Slovin, J. Rose, and D. Howard, "A 25 THz  $f_{CO}$  (6.3 fs  $t_{ON}$   $c_{OFF}$ ) phase-change material RF switch fabricated in a high volume manufacturing environment with demonstrated cycling > 1 billion times," in *Proc. IEEE/MTT-S Int. Microw. Symp.*, 2020, pp. 45–48.
- [51] A. Lebedev et al., "Influence of Se, Pb and Mn impurities on the ferroelectric phase transition in GeTe studied by EXAFS," *Phase Transitions*, vol. 60, no. 2, pp. 67–77, 1997.
- [52] E. I. Givargizov, A. Melnikova, and D. W. Wester, *Growth of Crystals*. New York, NY, USA: Springer, 1986.
- [53] R. Hein et al., "Superconductivity in germanium telluride," *Phys. Rev. Lett.*, vol. 12, no. 12, Art. no. 320, 1964.
- [54] E. K. Chua, "Development of phase change switches with low resistance in the 'ON' state," Ph.D. dissertation, Carnegie Mellon Univ., Pittsburgh, PA, USA, 2011.
- [55] P. Borodulin et al., "Recent advances in fabrication and characterization of GeTe-based phase-change RF switches and MMICs," in *Proc. IEEE MTT-S Int. Microw. Symp.*, Honolulu, HI, USA, 2017, pp. 285–288.
- [56] M. Wang and M. Rais-Zadeh, "Directly heated four-terminal phase change switches," in *Proc. IEEE MTT-S Int. Microw. Symp.*, Tampa, FL, USA, 2014, pp. 1–4.
- [57] M. Wang, Y. Shim, and M. Rais-Zadeh, "A low-loss directly heated two-port RF phase change switch," *IEEE Electron Device Lett.*, vol. 35, no. 4, pp. 491–493, Apr. 2014.
- [58] I. Bettoumi et al., "An integrated multiphysics model for phase-change material switches," in *Proc. IEEE 51st Eur. Microw. Conf.*, 2022, pp. 934–937.
- [59] M. Wang, F. Lin, and M. Rais-Zadeh, "Need a change? Try GeTe: A reconfigurable filter using germanium telluride phase change RF switches," *IEEE Microw. Mag.*, vol. 17, no. 12, pp. 70–79, Dec. 2016.
- [60] M. Wang and M. Rais-Zadeh, "Development and evaluation of germanium telluride phase change material based ohmic switches for RF applications," *J. Micromechanics Microeng.*, vol. 27, no. 1, 2017, Art. no. 013001.
- [61] N. El-Hinnawy et al., "Low-loss latching microw. switch using thermally pulsed non-volatile chalcogenide phase change materials," *Appl. Phys. Lett.*, vol. 105, no. 1, 2014, Art. no. 013501.
- [62] J.-S. Moon et al., "11 THz figure-of-merit phase-change RF switches for reconfigurable wireless front-ends," in *Proc. IEEE MTT-S Int. Microw. Symp.*, 2015, pp. 1–4.
- [63] J.-S. Moon, H.-C. Seo, and D. Le, "High linearity 1-ohm RF switches with phase-change materials," in *Proc. IEEE 14th Top. Meeting Silicon Monolithic Integr. Circuits RF Syst.*, 2014, pp. 7–9.
- [64] J.-S. Moon et al., "Phase-change RF switches with robust switching cycle endurance," in *Proc. IEEE Radio Wireless Symp.*, Anaheim, CA, USA, 2018, pp. 231–233.
- [65] T. Singh and R. R. Mansour, "Non-volatile multiport DC–30GHz monolithically integrated phase-change transfer switches," *IEEE Electron Device Lett.*, vol. 42, no. 6, pp. 867–870, Jun. 2021.
- [66] I. Bettoumi, N. L. Gall, and P. Blondy, "Phase change material (PCM) RF switches with integrated decoupling bias circuit," *IEEE Microw. Wireless Compon. Lett.*, vol. 32, no. 1, pp. 52–55, Jan. 2022.
- [67] M. R. King et al., "Connecting post-pulsing electrical and microstructural features in GeTe-based inline phase change switches," *J. Appl. Phys.*, vol. 124, no. 19, 2018, Art. no. 195103.
- [68] T. Singh, N. K. Khaira, and R. R. Mansour, "Monolithically integrated reconfigurable RF MEMS based impedance tuner on SOI substrate," in *Proc. IEEE MTT-S Int. Microw. Symp.*, Boston, MA, USA, 2019, pp. 790–792.
- [69] G. Slovin, N. El-Hinnawy, C. Masse, J. Rose, and D. Howard, "Multi-throw SPNT circuits using phase-change material RF switches for 5G and millimeter wave applications," in *Proc. IEEE MTT-S Int. Microw. Symp.*, 2021, pp. 428–430.
- [70] C. Hillman, P. A. Stupar, and Z. Griffith, "VO<sub>2</sub> switches for millimeter and submillimeter-wave applications," in *Proc. IEEE Compound Semiconductor Integr. Circuit Symp.*, New Orleans, LA, USA, 2015, pp. 1–4.
- [71] J.-S. Moon et al., "10.6 THz figure-of-merit phase-change RF switches with embedded micro-heater," in *Proc. IEEE 15th Top. Meeting Silicon Monolithic Integr. Circuits RF Syst.*, 2015, pp. 73–75.
- [72] F. Amin et al., "Wideband SPDT and SP4T RF switches using phase-change material in a SiGe BiCMOS process," in *Proc. IEEE MTT-S Int. Microw. Symp.*, 2021, pp. 431–434.
- [73] N. Wainstein, G. Ankonina, S. Kvatinsky, and E. Yalon, "Compact modeling and electrothermal measurements of indirectly heated phase-change RF switches," *IEEE Trans. Electron Devices*, vol. 67, no. 11, pp. 5182–5187, Nov. 2020.
- [74] D. Baltimas and G. M. Rebeiz, "A 25–50GHz phase change material (PCM) 5-bit true time delay phase shifter in a production SiGe BiCMOS process," in *Proc. IEEE MTT-S Int. Microw. Symp.*, 2021, pp. 435–437.



- [75] Y.-Y. Huang, W. Woo, Y. Yoon, and C.-H. Lee, "Highly linear RF CMOS variable attenuators with adaptive body biasing," *IEEE J. Solid-State Circuits*, vol. 46, no. 5, pp. 1023–1033, May 2011.
- [76] H. Dogan, R. G. Meyer, and A. M. Niknejad, "Analysis and design of RF CMOS attenuators," *IEEE J. Solid-State Circuits*, vol. 43, no. 10, pp. 2269–2283, Oct. 2008.
- [77] R. M. Young et al., "Improvements in gete-based phase change RF switches," in *Proc. IEEE/MTT-S Int. Microw. Symp.*, 2018, pp. 832–835.
- [78] D. Adler et al., "Threshold switching in chalcogenide-glass thin films," *J. Appl. Phys.*, vol. 51, no. 6, pp. 3289–3309, 1980.
- [79] R. Gu et al., "Structural features of chalcogenide glass SiTe: An ovonic threshold switching material," *APL Mater.*, vol. 9, no. 8, 2021, Art. no. 081101.
- [80] B. Song, H. Xu, S. Liu, H. Liu, and Q. Li, "Threshold switching behavior of Ag-SiTe-based selector device and annealing effect on its characteristics," *IEEE J. Electron Devices Soc.*, vol. 6, pp. 674–679, 2018.
- [81] Z. Zhang et al., "Improvement of resistive switching performance in sulfur-doped HfOx-based RRAM," *Materials*, vol. 14, no. 12, 2021, Art. no. 3330.
- [82] T. Kim et al., "Ovonic threshold switching in polycrystalline zinc telluride thin films deposited by RF sputtering," *Nanotechnol.*, vol. 30, no. 13, 2019, Art. no. 13LT01.
- [83] J. Zhao et al., "Role and optimization of thermal rapid annealing in Ta/TaOx/Ru based resistive switching memory," *Vacuum*, vol. 191, 2021, Art. no. 110392.
- [84] F. Morin, "Oxides of the 3D transition metals," *Bell Syst. Tech. J.*, vol. 37, no. 4, pp. 1047–1084, 1958.
- [85] J. B. Goodenough, "The two components of the crystallographic transition in VO<sub>2</sub>," *J. Solid State Chem.*, vol. 3, no. 4, pp. 490–500, 1971.
- [86] H. Futaki, "A new type semiconductor (critical temperature resistor)," *Jpn. J. Appl. Phys.*, vol. 4, no. 1, 1965, Art. no. 28.
- [87] S. Koide and H. Takei, "Epitaxial growth of VO<sub>2</sub> single crystals and their anisotropic properties in electrical resistivities," *J. Phys. Soc. Jpn.*, vol. 22, no. 3, pp. 946–947, 1967.
- [88] A. Barker Jr., H. Verleur, and H. Guggenheim, "Infrared optical properties of vanadium dioxide above and below the transition temperature," *Phys. Rev. Lett.*, vol. 17, no. 26, 1966, Art. no. 1286.
- [89] M. Imada, A. Fujimori, and Y. Tokura, "Metal-insulator transitions," *Rev. Modern Phys.*, vol. 70, no. 4, 1998, Art. no. 1039.
- [90] R. Cope and A. Penn, "High-speed solid-state thermal switches based on vanadium dioxide," *J. Phys. D, Appl. Phys.*, vol. 1, no. 2, 1968, Art. no. 161.
- [91] P. Hood and J. DeNatale, "Millimeter-wave dielectric properties of epitaxial vanadium dioxide thin films," *J. Appl. Phys.*, vol. 70, no. 1, pp. 376–381, 1991.
- [92] F. Dumas-Bouchiat et al., "RF-microwave switches based on reversible semiconductor-metal transition of VO<sub>2</sub> thin films synthesized by pulsed-laser deposition," *Appl. Phys. Lett.*, vol. 91, no. 22, 2007, Art. no. 223505.
- [93] A. Cavalleri et al., "Femtosecond structural dynamics in VO<sub>2</sub> during an ultrafast solid-solid phase transition," *Phys. Rev. Lett.*, vol. 87, no. 23, 2001, Art. no. 237401.
- [94] G. Stefanovich, A. Pergament, and D. Stefanovich, "Electrical switching and mott transition in VO<sub>2</sub>," *J. Phys., Condens. Matter*, vol. 12, no. 41, 2000, Art. no. 8837.
- [95] H. Jerominek, F. Picard, and D. Vincent, "Vanadium oxide films for optical switching and detection," *Opt. Eng.*, vol. 32, no. 9, pp. 2092–2099, 1993.
- [96] M. Li et al., "Hydrothermal synthesis of VO<sub>2</sub> polymorphs: Advantages, challenges and prospects for the application of energy efficient smart windows," *Small*, vol. 13, no. 36, 2017, Art. no. 1701147.
- [97] B. Hu et al., "External-strain induced insulating phase transition in VO<sub>2</sub> nanobeam and its application as flexible strain sensor," *Adv. Mater.*, vol. 22, no. 45, pp. 5134–5139, 2010.
- [98] V. R. Morrison et al., "A photoinduced metal-like phase of monoclinic VO<sub>2</sub> revealed by ultrafast electron diffraction," *Science*, vol. 346, no. 6208, pp. 445–448, 2014.
- [99] N. Shukla et al., "A steep-slope transistor based on abrupt electronic phase transition," *Nature Commun.*, vol. 6, no. 1, pp. 1–6, 2015.
- [100] D. Ruzmetov et al., "Three-terminal field effect devices utilizing thin film vanadium oxide as the channel layer," *J. Appl. Phys.*, vol. 107, no. 11, 2010, Art. no. 114516.
- [101] E. Sovero, D. Deakin, J. A. Higgins, J. F. DeNatale, and S. Pittman, "Fast thin film vanadium dioxide microwave switches," in *Proc. IEEE 12th Annu. Symp. Gallium Arsenide Integr. Circuit*, 1990, pp. 101–103.
- [102] M. Stotz, S.-D. Fritze, H. Downar, and J. Wenger, "Thermally controlled coplanar microwave switches," in *Proc. IEEE 29th Eur. Microw. Conf.*, 1999, vol. 2, pp. 415–418.
- [103] J. Givernaud, C. Champeaux, A. Catherinot, A. Pothier, P. Blondy, and A. Crunteanu, "Tunable band stop filters based on metal-insulator transition in vanadium dioxide thin films," in *Proc. IEEE MTT-S Int. Microw. Symp.*, 2008, pp. 1103–1106.
- [104] D. E. Anagnostou, D. Torres, T. S. Teeslink, and N. Sepulveda, "Vanadium dioxide for reconfigurable antennas and microwave devices: Enabling RF reconfigurability through smart materials," *IEEE Antennas Propag. Mag.*, vol. 62, no. 3, pp. 58–73, Jun. 2020.
- [105] A. Crunteanu et al., "Voltage-and current-activated metal-insulator transition in VO<sub>2</sub>-based electrical switches: A lifetime operation analysis," *Sci. Technol. Adv. Mater.*, vol. 11, 2010, Art. no. 065002.
- [106] S. D. Ha et al., "Electrical switching dynamics and broadband microwave characteristics of VO<sub>2</sub> radio frequency devices," *J. Appl. Phys.*, vol. 113, no. 18, 2013, Art. no. 184501.
- [107] M. Field et al., "Vanadium dioxide phase change switches," *Proc SPIE* vol. 9479, 2015, Art. no. 947908.
- [108] E. A. Casu et al., "Tunable RF phase shifters based on vanadium dioxide metal insulator transition," *IEEE J. Electron Devices Soc.*, vol. 6, pp. 965–971, 2018.
- [109] R. Yahiaoui and H. H. Ouslimani, "Broadband polarization-independent wide-angle and reconfigurable phase transition hybrid metamaterial absorber," *J. Appl. Phys.*, vol. 122, no. 9, 2017, Art. no. 093104.
- [110] S. Wang et al., "Tunable inductors using vanadium dioxide as the control material," *Microw. Opt. Techn. Lett.*, vol. 59, no. 5, pp. 1057–1061, 2017.
- [111] R. Cabrera, E. Merced, and N. Sepúlveda, "Performance of electrothermally driven VO<sub>2</sub>-based mems actuators," *J. Microelectromech. Syst.*, vol. 23, no. 1, pp. 243–251, 2013.
- [112] J. Jiang, K. W. Wong, and R. R. Mansour, "A VO<sub>2</sub>-based 30GHz variable attenuator," in *Proc. IEEE MTT-S Int. Microw. Symp.*, 2017, pp. 911–913.
- [113] R. Matos, A.-S. Kaddour, S. V. Georgakopoulos, and N. Pala, "Reflectarrays with ultra-reconfigurable VO<sub>2</sub> unit-cells for next-generation communication systems," in *Proc. IEEE Texas Symp. Wireless Microw. Circuits Syst.*, 2021, pp. 1–5.
- [114] R. Matos and N. Pala, "VO<sub>2</sub>-based ultra-reconfigurable intelligent reflective surface for 5G applications," *Sci. Rep.*, vol. 12, no. 1, pp. 1–9, 2022.
- [115] M. Vaseem et al., "Development of VO<sub>2</sub>-nanoparticle-based metal-insulator transition electronic ink," *Adv. Electron. Mater.*, vol. 5, no. 5, 2019, Art. no. 1800949.
- [116] Z. Su, M. Vaseem, S. Yang, K. Klionovski, and A. Shamim, "Fully printed VO<sub>2</sub> switch based reconfigurable PIFA antenna," in *Proc. IEEE Int. Symp. Antennas Propag. USNC/URSI Nat. Radio Sci. Meeting*, 2018, pp. 1683–1684.
- [117] S. Yang, M. Vaseem, and A. Shamim, "Fully inkjet-printed VO<sub>2</sub>-based radio-frequency switches for flexible reconfigurable components," *Adv. Mater. Technol.*, vol. 4, no. 1, 2019, Art. no. 1800276.
- [118] S. Yang, W. Li, M. Vaseem, and A. Shamim, "Additively manufactured dual-mode reconfigurable filter employing VO<sub>2</sub>-based switches," *IEEE Trans. Compon. Packag. Manuf. Technol.*, vol. 10, no. 10, pp. 1738–1744, Oct. 2020.
- [119] W. Li et al., "Flexible and reconfigurable radio frequency electronics realized by high-throughput screen printing of vanadium dioxide switches," *Microsyst. Nanoeng.*, vol. 6, no. 1, pp. 1–12, 2020.
- [120] A. Crunteanu et al., "Voltage-and current-activated metal-insulator transition in VO<sub>2</sub>-based electrical switches: A lifetime operation analysis," *Sci. Technol. Adv. Mater.*, vol. 11, 2010, Art. no. 065002.
- [121] J. Leroy et al., "High-speed metal-insulator transition in vanadium dioxide films induced by an electrical pulsed voltage over nano-gap electrodes," *Appl. Phys. Lett.*, vol. 100, no. 21, 2012, Art. no. 213507.
- [122] S. D. Ha, Y. Zhou, C. J. Fisher, S. Ramanathan, and J. P. Treadway, "Abrupt insertion loss drop by RF-triggering of the phase transition in VO<sub>2</sub> CPW switches," *IEEE Microw. Wireless Compon. Lett.*, vol. 24, no. 8, pp. 575–577, Aug. 2014.

- [123] C. Hillman, P. A. Stupar, J. B. Hacker, Z. Griffith, M. Field, and M. Rodwell, "An ultra-low loss millimeter-wave solid state switch technology based on the metal-insulator-transition of vanadium dioxide," in *Proc. IEEE MTT-S Int. Microw. Symp.*, 2014, pp. 1–4.
- [124] T. S. Teeslink, D. Torres, J. L. Ebel, N. Sepulveda, and D. E. Anagnostou, "Reconfigurable bowtie antenna using metal-insulator transition in vanadium dioxide," *IEEE Antennas Wireless Propag. Lett.*, vol. 14, pp. 1381–1384, 2015.
- [125] L. Huitema et al., "Highly integrated VO<sub>2</sub>-based tunable antenna for millimeter-wave applications," *Appl. Phys. Lett.*, vol. 110, no. 20, 2017, Art. no. 203501.
- [126] B. Gerislioglu et al., "VO<sub>2</sub>-based reconfigurable antenna platform with addressable microheater matrix," *Adv. Electron. Mat.*, vol. 3, no. 9, 2017, Art. no. 1700170.
- [127] G.-B. Liu et al., "A dual-band and wideband omnidirectional circularly polarized antenna based on VO<sub>2</sub>," *Int. J. RF Microw. Comput.-Aided Eng.*, vol. 29, no. 3, 2019, Art. no. e21676.
- [128] H.-F. Zhang et al., "Design of a tunable omnidirectional circularly polarized antenna based on VO<sub>2</sub>," *Int. J. RF Microw. Comput.-Aided Eng.*, vol. 30, no. 1, 2020, Art. no. e21997.
- [129] W. Yang, C. Zhou, Q. Xue, Q. Wen, and W. Che, "Millimeter-wave frequency-reconfigurable metasurface antenna based on vanadium dioxide films," *IEEE Trans. Antennas Propag.*, vol. 69, no. 8, pp. 4359–4369, Aug. 2021.
- [130] D. E. Anagnostou et al., "Integration of resistive heaters for phase-change reconfigurable antennas," in *Proc. 11th Eur. Conf. Antennas Propag.*, 2017, pp. 2349–2350.
- [131] Z. Su, M. Vaseem, W. Li, S. Yang, and A. Shamim, "Additively manufactured frequency/radiation pattern reconfigurable antenna based on monolithically printed VO<sub>2</sub> switch," in *Proc. IEEE 13th Eur. Conf. Antennas Propag.*, 2019, pp. 1–4.
- [132] W. A. Vitale et al., "Electrothermal actuation of vanadium dioxide for tunable capacitors and microwave filters with integrated microheaters," *Sensors Actuators A, Phys.*, vol. 241, pp. 245–253, 2016.
- [133] E. A. Casu et al., "Vanadium oxide bandstop tunable filter for Ka frequency bands based on a novel reconfigurable spiral shape defected ground plane CPW," *IEEE Access*, vol. 6, pp. 12206–12212, 2018.
- [134] A. O. Suleiman et al., "Tuning VO<sub>2</sub> phase stability by a combined effect of Cr doping and oxygen pressure," *Appl. Surf. Sci.*, vol. 571, 2022, Art. no. 151267.



**TEJINDER SINGH** (Senior Member, IEEE) received the Ph.D. degree (with highest academic honor) in electrical and computer engineering from the University of Waterloo, Waterloo, ON, Canada, in 2020. He is currently a Principal Member of Technical Staff with the Advanced Wireless Technology R&D Group, Office of the CTO, Dell Technologies, Ottawa, ON, and an Adjunct Professor with the University of Waterloo. He was a Postdoctoral Fellow with NASA Jet Propulsion Laboratory, California Institute of Technology (Caltech), Pasadena, CA, USA, from 2020 to 2021 and a Research Assistant Professor with the University of Waterloo from 2020 to 2022. He has authored or coauthored several research publications in the areas of phase-change materials (PCMs), microelectromechanical systems (MEMS), low temperature superconducting (LTS) quantum devices, and reconfigurable intelligent surfaces (RIS) for B5G/6G applications. He was the recipient of the Governor General's Gold Medal, one of the highest Canadian honors for his academic excellence and outstanding doctoral research. He has received highly competitive and prestigious federal awards from the Government of Canada including Vanier Canada Scholarship from 2017 to 2020 and the NSERC Postdoctoral Fellowship from 2020 to 2022. He also received the competitive Waterloo Institute for Nanotechnology (WIN) Nanofellowship (twice) in 2017–2018. His research contributions have bestowed numerous accolades including the Brian L. Barge Microsystems Integration Award from Canada Microsystems (CMC) in 2019, the Young Engineer Award from the European Microwave Association (EuMA) in 2021, and more than ten Best Paper Awards at several prestigious international conferences. He is currently an Associate Editor for IEEE TRANSACTIONS ON MICROWAVE THEORY AND TECHNIQUES, and *Microsystem Technologies* (Springer-Nature), the Editor of IEEE MTT-S Newsletter, and Technical Paper Review Committee Member of the IEEE MTT-S International Microwave Symposium (IMS).



Technologies. She specializes in piezoelectrics and phase change materials.



of Science and Technology, Thuwal, Saudi Arabia, where he is currently a Research Scientist. He has more than 12 years of experience in material preparation and ink-formulation for printed electronics. For the last six years, his focus has been on functional ink-materials for RF electronics and sensor. He has developed magnetic and VO<sub>2</sub>-based ink-materials for fully-printed reconfigurable and tunable applications. He has authored more than 60 publications, three book chapters, five patents, and 80 research paper presentations in several national and international conferences.



KAUST, where he is currently an Associate Professor and Principal investigator of the IMPACT Lab. He was an invited Researcher with the VTT Micro-Modules Research Center, Oulu, Finland, in 2006. He was the recipient of best paper awards in IEEE IMS 2016, IEEE MECAP 2016, IEEE EuWIT 2008; first prize in the IEEE IMS 2019 3MT competition; finalist/honorable mention prizes in IEEE APS Design Competition 2020, IEEE APS 2005, IEEE IMS 2014, IEEE IMS 2017 (3MT competition); and R. W. P. King IEEE Award for journal papers in IEEE TAP 2017 and 2020. He was given the Ottawa Centre of Research Innovation (OCRI) Researcher of the Year Award in 2008 in Canada. His work on wireless dosimeter won the ITAC SMC Award at Canadian Microelectronics TEXPO in 2007. Prof. Shamim also was the recipient of numerous business-related awards, including 1st Prize in Canada's national business plan competition and was awarded OCRI Entrepreneur of the Year Award in 2010 and the Kings Prize for the best innovation of the year (2018) for his work on sensors for the oil industry. He is an author of one book, three book chapters, and 250 publications; an inventor on 30 patents; and has given 70 invited talks at various international forums. His research interests include innovative antenna designs and their integration strategies with circuits and sensors for flexible and wearable wireless sensing systems through a combination of CMOS and additive manufacturing technologies. Dr. Shamim is a Member of the IEEE APS Measurements Committee and the IEEE MTT Microwave Control Techniques Committee, founded the first IEEE AP/MTT chapter in Saudi Arabia (2013) and served on the editorial board of IEEE TRANSACTIONS ON ANTENNAS AND PROPAGATION (2013–2019), and as the Guest Editor for IEEE AWPL Special issue (2019). He is currently an Associate Editor for IEEE JOURNAL OF ELECTROMAGNETICS, RF AND MICROWAVES IN MEDICINE AND BIOLOGY.

**GWENDOLYN HUMMEL** (Member, IEEE) received the B.S. degree in electrical engineering from the Illinois Institute of Technology, Chicago, IL, USA, in 2013, the M.S. degree in electrical and computer engineering from Northeastern University, Boston, MA, USA, in 2015, and the Ph.D. degree in electrical engineering, with specialization in microfabrication, materials, and devices from Northeastern University, in 2018. She is currently a Senior Member of Technical Staff with Sandia National Laboratories, Department of MEMS

**MOHAMMAD VASEEM** (Member, IEEE) received the M.Sc. degree in physical chemistry from Aligarh Muslim University, Aligarh, India, in 2005, and the Ph.D. degree in chemical engineering from Chonbuk National University, Jeonju, South Korea, in 2011. From 2011 to 2014, he was a Postdoctoral Fellow with World Class University Project and Brain Korea 21 Project with Chonbuk National University. From 2015 to 2018, he was a Postdoctoral Fellow with the Electrical Engineering Program with the King Abdullah University of Science and Technology, Thuwal, Saudi Arabia, where he is currently a Research Scientist. He has more than 12 years of experience in material preparation and ink-formulation for printed electronics. For the last six years, his focus has been on functional ink-materials for RF electronics and sensor. He has developed magnetic and VO<sub>2</sub>-based ink-materials for fully-printed reconfigurable and tunable applications. He has authored more than 60 publications, three book chapters, five patents, and 80 research paper presentations in several national and international conferences.

**ATIF SHAMIM** (Senior Member, IEEE) received the M.S. and Ph.D. degrees in electrical engineering from Carleton University, Ottawa, ON, Canada, in 2004 and 2009, respectively. He was an NSERC Alexander Graham Bell Graduate Scholar with Carleton University from 2007 to 2009 and an NSERC postdoctoral Fellow in 2009–2010 with Royal Military College Canada and the King Abdullah University of Science and Technology (KAUST), Thuwal, Saudi Arabia. In August 2010, he joined the Electrical Engineering Program,